PHYSICAL REVIEW B **79**, 235321 (2009)

Critical behavior of a point contact in a quantum spin Hall insulator

Jeffrey C. Y. Teo and C. L. Kane
Department of Physics and Astronomy, University of Pennsylvania, Philadelphia, Pennsylvania 19104, USA
(Received 20 April 2009; published 18 June 2009)

We study a quantum point contact in a quantum spin Hall insulator. It has recently been shown that the Luttinger liquid theory of such a structure maps to the theory of a weak link in a Luttinger liquid with spin with Luttinger liquid parameters $g_\rho = 1/g_\sigma = g < 1$. We show that for weak interactions, $1/2 < g < 1$, the pinch-off of the point contact as a function of gate voltage is controlled by a novel quantum critical point, which is a realization of a nontrivial intermediate fixed point found previously in the Luttinger liquid model with spin. We predict that the dependence of the conductance on gate voltage near the pinch-off transition for different temperatures collapses onto a universal curve described by a crossover scaling function associated with that fixed point. We compute the conductance and critical exponents of the critical point as well as the universal scaling function in solvable limits, which include $g = 1 - \epsilon$, $g = 1/2 + \epsilon$, and $g = 1/\sqrt{3}$. These results, along with a general scaling analysis, provide an overall picture of the critical behavior as a function of g. In addition, we analyze the structure of the four-terminal conductance of the point contact in the weak tunneling and weak backscattering limits. We find that different components of the conductance can have different temperature dependences. In particular, we identify a skew conductance G_{XY}, which we predict vanishes as T^γ with $\gamma \geq 2$. This behavior is a direct consequence of the unique edge state structure of the quantum spin Hall insulator. Finally, we show that for strong interactions, $g < 1/2$, the presence of spin nonconserving spin-orbit interactions leads to a novel time-reversal-symmetry breaking insulating phase. In this phase, the transport is carried by spinless chargons and chargeless spinons. These lead to nontrivial correlations in the low frequency shot noise. Implications for experiments on HgCdTe quantum well structures will be discussed.

DOI: 10.1103/PhysRevB.79.235321 PACS number(s): 71.10.Pm, 72.15.Nj, 85.75.−d

I. INTRODUCTION

A quantum spin Hall insulator (QSHI) is a time-reversal invariant two-dimensional electronic phase which has a bulk energy gap generated by the spin-orbit interaction.[1,2] It has a topological order[3] which requires the presence of gapless edge states similar to those that occur in the integer quantum Hall effect. In the simplest version, the QSHI can be understood as two time reversed copies of the integer quantum Hall state[4] for up and down spins. The edge states, which propagate in opposite directions for the two spins, form a unique one-dimensional (1D) system in which elastic backscattering is forbidden by time-reversal symmetry.[1] This state occurs in HgCdTe quantum well structures,[5] and experiments have verified the basic features of the edge states, including the Landauer conductance[6] $2e^2/h$, as well as the nonlocality of the edge state transport.[7]

In the presence of electron interactions, the edge states form a Luttinger liquid.[8–14] For strong interactions (when the Luttinger liquid parameter $g < 3/8$) random two particle backscattering processes destabilize the edge states, leading to an Anderson localized phase. For $g > 3/8$ (or a sufficiently clean system), however, one expects the characteristic power-law behavior for tunneling of a Luttinger liquid.

A powerful tool for probing edge state transport experimentally is to make a quantum point contact. As depicted in Figs. 1(a) and 1(b), a gate voltage controls the coupling between edge states on either side of a Hall bar as the point contact is pinched off. Recently, the point contact problem for a QSHI has been studied.[10,11] Hou *et al.*[10] made the interesting observation that the QSHI problem maps to an earlier studied model[15,16] of a weak link in a spinful Luttinger liquid (SLL), in which the charge and spin Luttinger parameters are given by $g_\rho = g$ and $g_\sigma = 1/g$.[17] For sufficiently strong interactions ($g < 1/2$) they found that the simple perfectly transmitting and perfectly reflecting phases are both unstable. They showed that as long as spin is conserved at the junction the low energy behavior is dominated by a non-

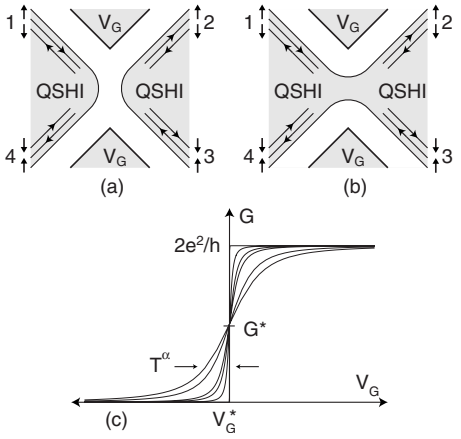

FIG. 1. A quantum point contact in a QSHI, controlled by a gate voltage V_G. In (a) $V_G < V_G^*$ and the point contact is pinched off. The spin filtered edge states are perfectly reflected. In (b) $V_G > V_G^*$ and the point contact is open. The edge states are perfectly transmitted. In (c) we plot the conductance (later defined as G_{XX}) as a function of V_G for different temperatures. As the temperature is lowered, the pinch-off curve sharpens up with a width T^α. The curves cross at a critical conductance G^*, and the shape of the curve has the universal scaling form (1.1). The plotted curves are based on Eq. (3.9), valid for $g = 1 - \epsilon$, which is computed in Sec. III C.

trivial "mixed" fixed point of the SLL, in which charge is reflected but spin is perfectly transmitted. This charge insulator/spin conductor (IC) phase leads to a novel structure in the four-terminal conductance of the point contact.

In this paper, we will focus on the QSHI point contact for weaker interactions when $1/2<g<1$. In this regime the open limit (or weak backscattering, "small v") and the pinched-off limit (or weak tunneling, "small t") are *both* stable perturbatively. This is different from the behavior in an ordinary Luttinger liquid[15,16,18] or a fractional quantum Hall point contact.[19,20] In those cases the perfectly transmitting limit is unstable for $g<1$. Weak backscattering is relevant and grows at low energy, leading to a crossover to the stable perfectly reflecting fixed point. The fact that both the small v and the small t limits are stable for the QSHI point contact means that there must be an intermediate unstable fixed point which separates the flows to the two limits. This unstable fixed point describes a quantum critical point where the point contact switches on as a function of the pinch-off gate voltage. We will argue that in the limit of zero temperature the point contact switches on abruptly as a function of gate voltage V_G, with conductances $G=0$ for $V_G<V_G^*$ and $G=2e^2/h$ for $V_G>V_G^*$. At finite but low temperature T, the shape of the pinch-off curve $G(V_G,T)$ is controlled by the crossover between the unstable and stable fixed points and is described by a universal crossover scaling function,

$$\lim_{\Delta V_G,T\to 0} G(V_G,T)=\frac{2e^2}{h}\mathcal{G}_g\left(c\frac{\Delta V_G}{T^{\alpha_g}}\right). \tag{1.1}$$

Here $\Delta V_G=V_G-V_G^*$ and c is a nonuniversal constant. α_g is a critical exponent describing the unstable intermediate fixed point. $\mathcal{G}_g(X)$ is a universal function which crosses over between 0 and 1 as a function of X. α_g and $\mathcal{G}_g(X)$ are completely determined by the Luttinger liquid parameter g. This behavior means that as temperature is lowered, the pinch-off curve as a function of V_G sharpens up with a characteristic width which vanishes as T^{α_g}, as shown schematically in Fig. 1(c). The curves at different low temperatures cross at $G_g^*=\mathcal{G}_g(0)$, the conductance of the critical point. Equation (1.1) predicts that data from different temperatures can be rescaled to lie on the same universal curve.

The crossover scaling function $\mathcal{G}_g(X)$ is similar to the scaling function that controls the line shape of resonances in a Luttinger liquid[16,21] and in a fractional quantum Hall point contact.[19] That scaling function was computed exactly for all g by Fendley *et al.*[22] using the thermodynamic Bethe ansatz. That problem, however, was simpler than ours because the critical point occurs at the weak backscattering limit, which is described by a boundary conformal field theory with a trivial boundary condition.[23] The intermediate fixed point relevant to our problem has no such simple description. Thus, even the critical point properties α_g and G_g^* (which were simple for the resonance problem) are highly nontrivial to determine.

Intermediate fixed points in Luttinger liquid problems were first discussed in Refs. 15 and 16 in the context of SLLs. However, for that problem they occur in a rather unphysical region of parameter space $g_\sigma>2$ because spin rotational invariance requires $g_\sigma=1$. The QSHI point contact provides a physically viable system to directly probe these nontrivial fixed points.

The existence of the intermediate fixed points can be inferred from the stability of the simple perfectly transmitting or reflecting fixed points.[15,16] However their properties are difficult to compute, and a general characterization of these critical points remains an unsolved problem in conformal field theory.[24] Two approaches have been used to study their properties. In Ref. 16, a perturbative approach was introduced which applies when the Luttinger parameters are close to their critical values g_σ^* and g_ρ^*, where the simple fixed points become unstable. (For instance, for the weak backscattering limit, $g_\rho^*=1/2$, $g_\sigma^*=3/2$.) For $g_{\rho,\sigma}=g_{\rho,\sigma}^*-\epsilon$, the fixed point is accessible in perturbation theory about the simple fixed point, and its properties can be computed in a manner analogous to the ϵ expansion in statistical mechanics.

An alternative approach is to map the theory for specific values of g_ρ and g_σ onto solvable models. In Ref. 25, Yi and Kane recast the Luttinger liquid barrier problem as a problem of quantum Brownian motion (QBM) in a two-dimensional periodic potential. When $g_\rho=1/3$, $g_\sigma=1$ and the potential has minima with a honeycomb lattice symmetry, a stable intermediate fixed point which occurs in that problem was identified with that of the three-channel Kondo problem. This, in turn, is related to the solvable $SU(2)_3$ Wess-Zumino-Witten model,[26] allowing for a complete characterization of the fixed point. This idea was further developed by Affleck *et al.*,[24] who provided a more general characterization of the fixed point in terms of the boundary conformal field theory of the three-state Pott's model. For $g_\rho=1/\sqrt{3}$ and $g_\sigma=\sqrt{3}$ the QBM model with triangular lattice symmetry has an unstable intermediate fixed point, which we will see is related to the fixed point of the QSHI problem. In Ref. 25 symmetry arguments were exploited to determine the critical conductance G^* in that case.

In this paper we will compute α_g and $\mathcal{G}_g(X)$ (along with a multiterminal generalization of the conductance) in three solvable limits:

(i) For $g=1-\epsilon$, we will perform an expansion for weak electron interactions. For noninteracting electrons the point contact can be characterized in terms of a scattering matrix S_{ij} for arbitrary transmission. Weak interactions lead to a logarithmic renormalization of S_{ij}. Following the method developed by Matveev *et al.*,[27] this allows $\mathcal{G}_g(X)$ and α_g to be calculated exactly in the limit $g\to 1$.

(ii) For $g=1/2+\epsilon$, we find that the intermediate fixed point approaches the charge insulator/spin conductor fixed point, allowing for a perturbative calculation of the fixed point properties G_g^* and α_g to leading order in ϵ. Moreover, for $g=1/2$ the Luttinger liquid theory can be fermionized, which allows the full crossover function $\mathcal{G}_g(X)$ to be determined in that limit.

(iii) For $g=1/\sqrt{3}$, the self-duality argument developed in Ref. 25 allows us to compute the fixed point conductance G^* exactly.

These three results, along with the general scaling analysis, provide an overall picture of the critical behavior of the QSHI point contact as a function of g.

In addition to the analysis of the pinch-off transition discussed above, we will touch on two other issues in this paper.

First, we will introduce a convenient parametrization of the four-terminal conductance as a 3×3 conductance matrix. In this form symmetry constraints on the conductance are reflected in a natural way. Moreover, we will predict that different components of the conductance matrix have different temperature dependences at the low temperature fixed points. In particular, we will introduce a "skew" conductance G_{XY}, which is predicted to vanish as T^{γ} with $\gamma \geq 2$. For noninteracting electrons we will show that $G_{XY}=0$ and for weak interactions $\gamma=2$. This behavior is a direct consequence of the spin filtered nature of the edge states and does not occur in a generic four-terminal conductance device. It is thus a powerful diagnostic for the edge states.

Second, we will examine the role of spin-orbit terms at the point contact which respect time-reversal symmetry but violate spin conservation. For $g>1/2$ we will provide evidence that such terms are *irrelevant* at the intermediate critical fixed point, so that they are unimportant for the critical behavior of the point contact. However, for $g<1/2$, such terms are relevant. Hou *et al.*[10] pointed out that these terms are relevant perturbations at the charge insulator/spin conductor fixed point for $g<1/2$, but they did not identify the stable phase to which the system flows at low energy. We will argue that the system flows to a time-reversal-symmetry breaking insulating state in which the *four-terminal* conductance $G_{ij}=0$. Since spin-orbit interaction terms will generically be present in a point contact, the true low energy behavior of a point contact will be described by this phase. An interesting consequence of the broken time-reversal symmetry of this phase is that the weak tunneling processes which dominate the conductance at low but finite temperature are not electron tunneling processes. Rather, they involve the tunneling of neutral spinons and spinless chargons. This has nontrivial implications for four-terminal noise correlation measurements. A related effect has been predicted by Maciejko *et al.*[12] for the insulating state of a single impurity on a single edge of a QSHI. This insulating state, however, requires stronger electron-electron interactions. It occurs in the regime $g<1/4$, where weak disorder already leads to Anderson localization.

This paper is organized as follows. In Sec. II we discuss our model and analyze five stable phases. In addition to the simple fixed points, where charge and spin are either perfectly reflected or perfectly transmitted, we discuss the time-reversal-symmetry breaking insulating phase which occurs for strong interactions with spin orbit. In Sec. III we discuss the critical behavior of the conductance at the pinch-off transition. We will begin in Sec. III A with a general discussion of the scaling theory and phase diagram along with a summary of our results. Readers who are not interested in the detailed calculations can go directly to this section. In the following sections we describe the calculations for $g=1/\sqrt{3}$, $g=1-\epsilon$, and $g=1/2+\epsilon$ in detail. In Sec. IV we conclude with a discussion of experimental and theoretical issues raised by this work. In the Appendix we describe our parametrization of the four-terminal conductance and show that in this representation symmetry constraints have a simple form.

II. MODEL AND STABLE PHASES

In this section we will describe the Luttinger liquid theory of the QSHI point contact. We will begin in Sec. II A by describing the Luttinger liquid model first for a single edge and then relating the four edges to the theory of the SLL. We then discuss the four-terminal conductance. In Sec. II B we describe the simple limits of our model which correspond to stable phases. The simplest limits are the perfect transmission limit or charge conductor/spin conductor (CC) and the perfect reflection limit or charge insulator/spin insulator (II). In addition we will discuss the "mixed" phases, including the IC and the charge conductor/spin insulator (CI).

For most of this section we will assume that spin is conserved. While spin nonconserving spin-orbit interactions are allowed and will generically be present we will argue that they are irrelevant for the fixed points and crossovers of physical interest. An exception to this, however, occurs for strong interactions when $g<1/2$. This will be discussed in Sec. II B 5, where we will show that there are relevant spin-orbit terms which destabilize the CC, II, and IC phases. We will argue that these perturbations flow to a different low temperature phase, which we identify as a time-reversal-symmetry breaking insulator (TBI). In that section we will explore the transport properties of that state.

Much of the theory presented in this section is contained either explicitly or implicitly in the work of Hou *et al.*,[10] as well as in Refs. 11, 15, and 16. We include it here to establish our notation and to make our discussion self-contained. We will highlight, however, three results of this section which are original to this work. They include (1) our analysis of the four-terminal conductance, which predicts that different components of the conductance matrix have different temperature dependences. In particular, we find that the skew conductance G_{XY} vanishes at low temperature as T^{γ} with $\gamma \geq 2$. (2) In Sec. II B 5 we introduce the TBI phase discussed above. (3) We introduce a perturbative analysis of the IC and CI phases in Secs. II B 3 and II B 4. While this was partially discussed in Ref. 16, we will show that a full analysis requires the introduction of a pseudospin degree of freedom in the perturbation theory. This new pseudospin does not affect the lowest order stability analysis of the IC phase, but it will prove crucial for the second-order renormalization group flows, which will be used in the ϵ expansion in Sec. III D.

A. Model

The edge states on the four edges in Figs. 1(a) and 1(b) emanating from the point contact may be described by the Hamiltonian

$$H_0 = \sum_{i=1}^{4} \int_0^{\infty} dx_i \mathcal{H}_0^i, \tag{2.1}$$

with

$$\mathcal{H}_0^i = iv_0(\psi_{i,\mathrm{in}}^{\dagger}\partial_x\psi_{i,\mathrm{in}} - \psi_{i,\mathrm{out}}^{\dagger}\partial_x\psi_{i,\mathrm{out}}) + u_2\psi_{i,\mathrm{in}}^{\dagger}\psi_{i,\mathrm{in}}\psi_{i,\mathrm{out}}^{\dagger}\psi_{i,\mathrm{out}} + \frac{1}{2}u_4[(\psi_{i,\mathrm{in}}^{\dagger}\psi_{i,\mathrm{in}})^2 + (\psi_{i,\mathrm{out}}^{\dagger}\psi_{i,\mathrm{out}})^2]. \tag{2.2}$$

Here $\psi_{i,\mathrm{in}}$ and $\psi_{i,\mathrm{out}}$ are a time reversed pair of fermion operators with opposite spin which propagate toward and away from the junction. v_0 is the bare Fermi velocity and u is

electron interaction strength. u_2 and u_4 are forward scattering interaction parameters. The boundary condition on the fermions at $x=0$ is determined by the transmission of the point contact and will be discussed in various limits below.

1. Bosonization of a single edge

We first consider the Luttinger liquid theory for a single edge. We thus bosonize according to

$$\psi_{i,a} = \frac{1}{\sqrt{2\pi x_c}} e^{i\phi_{i,a}}, \tag{2.3}$$

where $a=\text{in},\text{out}$ and x_c is a short distance cutoff. $\psi_{i,a}$ obey the Kac Moody commutation algebra,

$$[\phi_{i,a}(x), \phi_{j,b}(y)] = i\pi\delta_{ij}\tau^z_{ab}\,\text{sgn}(x-y). \tag{2.4}$$

Then,

$$\mathcal{H}_0^i = \frac{v_0}{4\pi}\{(1+\lambda_4)[(\partial_x\phi_{i,\text{in}})^2 + (\partial_x\phi_{i,\text{out}})^2] - 2\lambda_2\partial_x\phi_{i,\text{in}}\partial_x\phi_{i,\text{out}}\}, \tag{2.5}$$

where $\lambda_i = u_i/(2\pi v_0)$. Changing variables

$$\begin{pmatrix}\phi_{i,\text{in}}\\ \phi_{i,\text{out}}\end{pmatrix} = \frac{1}{2g}\begin{pmatrix}1+g & 1-g\\ 1-g & 1+g\end{pmatrix}\begin{pmatrix}\tilde{\phi}_{i,\text{in}}\\ \tilde{\phi}_{i,\text{out}}\end{pmatrix} \tag{2.6}$$

transforms Eq. (2.5) into a theory of decoupled chiral bosons,

$$\mathcal{H}_0 = \frac{v}{4\pi g}[(\partial_x\tilde{\phi}_{i,\text{in}})^2 + (\partial_x\tilde{\phi}_{i,\text{out}})^2], \tag{2.7}$$

where $\tilde{\phi}_{i,a}$ obey

$$[\tilde{\phi}_{i,a}(x), \tilde{\phi}_{j,b}(y)] = i\pi g\,\delta_{ij}\tau^z_{ab}\,\text{sgn}(x-y). \tag{2.8}$$

Here $v = v_0\sqrt{(1+\lambda_4)^2-\lambda_2^2}$ and

$$g = \sqrt{\frac{1+\lambda_4-\lambda_2}{1+\lambda_4+\lambda_2}}. \tag{2.9}$$

The Luttinger liquid parameter g determines the power-law exponents for various quantities. For instance, the tunneling density of states scales as $\rho(E) \propto E^{(g+1/g)/2-1}$.

2. Mapping to spinful Luttinger liquid

Consider an open point contact in a Hall bar geometry with edge states on the top and bottom edges which continuously connect leads 1 and 2 and leads 3 and 4. We then define left and right moving fields with spin $\uparrow,\downarrow$ as

$$\begin{aligned}
\phi_{R\uparrow} &= \phi_{1,\text{in}}(-x)\,\theta(-x) + \phi_{2,\text{out}}(x)\,\theta(x),\\
\phi_{L\downarrow} &= \phi_{2,\text{in}}(x)\,\theta(x) + \phi_{1,\text{out}}(-x)\,\theta(-x),\\
\phi_{L\uparrow} &= \phi_{3,\text{in}}(x)\,\theta(x) + \phi_{4,\text{out}}(-x)\,\theta(-x),\\
\phi_{R\downarrow} &= \phi_{4,\text{in}}(-x)\,\theta(-x) + \phi_{3,\text{out}}(x)\,\theta(x).
\end{aligned} \tag{2.10}$$

It is then useful to define sum and difference fields as

TABLE I. The effect of discrete symmetry operations on the boson fields θ_ρ and θ_σ.

O	$\Theta O\Theta^{-1}$	$\mathcal{M}_X O\mathcal{M}_X^{-1}$	$\mathcal{M}_Y O\mathcal{M}_Y^{-1}$
θ_ρ	θ_ρ	$-\theta_\rho$	θ_ρ
φ_ρ	$-\varphi_\rho$	φ_ρ	φ_ρ
θ_σ	$-\theta_\sigma$	θ_σ	$-\theta_\sigma$
φ_σ	$\varphi_\sigma+\pi$	$-\varphi_\sigma$	$-\varphi_\sigma$

$$\phi_{a\sigma} = \frac{1}{2}(\varphi_\rho + \sigma\varphi_\sigma + a\theta_\rho + a\sigma\theta_\sigma), \tag{2.11}$$

where $a=R,L=+,-$ and $\sigma=\uparrow,\downarrow=+,-$. Then, θ_α and ϕ_α obey

$$[\theta_\alpha(x), \phi_\beta(y)] = 2\pi i\,\delta_{\alpha\beta}\theta(x-y), \tag{2.12}$$

and Eqs. (2.3) and (2.5) become[10]

$$H_0 = \int_{-\infty}^{\infty} dx \sum_{a=\sigma,\rho} \frac{v}{4\pi}\left[g_a(\partial_x\varphi_a)^2 + \frac{1}{g_a}(\partial_x\theta_a)^2\right], \tag{2.13}$$

where

$$g_\rho = g, \quad g_\sigma = 1/g, \tag{2.14}$$

and g and v are given in Sec. II A 1.

It is useful to list the effect of symmetry operations on the charge-spin variables because symmetries constrain the allowed tunneling operators. Charge conservation leads to gauge invariance under the transformation $\phi_\rho \to \phi_\rho + \delta_\rho$. The conservation of spin S_z leads to invariance under $\phi_\sigma \to \phi_\sigma + \delta_\sigma$. The effects of time-reversal and mirror symmetries are shown in Table I. Time-reversal symmetry is specified by the operation $\Theta\psi_{a\sigma}\Theta^{-1} = i\sigma\psi_{\bar{a}\bar{\sigma}}$. The mirror $\mathcal{M}_X$ interchanges leads $14 \leftrightarrow 23$ while $\mathcal{M}_Y$ interchanges leads $12 \leftrightarrow 34$.

3. Four-terminal conductance

The central measurable quantity is the four-terminal conductance, defined by

$$I_i = \sum_j G_{ij}V_j, \tag{2.15}$$

where I_i is the current flowing into lead i. G_{ij} is in general characterizing by nine independent parameters. In the Appendix we introduce a convenient representation for these parameters, which simplifies the representation of symmetry constraints. Here we will summarize the key points of that analysis.

The presence of both time-reversal symmetry and spin conservation considerably simplifies the conductance. It is characterized by *three* independent conductances,

$$\begin{pmatrix}I_X\\ I_Y\end{pmatrix} = \begin{pmatrix}G_{XX} & G_{XY}\\ G_{YX} & G_{YY}\end{pmatrix}\begin{pmatrix}V_X\\ V_Y\end{pmatrix}. \tag{2.16}$$

Here $I_X = I_1 + I_4$ is the current flowing from left to right in Fig. 1, while $I_Y = I_1 + I_2$ is the current flowing from top to bottom. Similarly, V_X is a voltage biasing lead (2.14) relative to Eq.

(2.23) and V_Y biases lead (2.12) relative to Eq. (2.34). G_{XX} is thus the *two-terminal* conductance measured horizontally, while G_{YY} is the two-terminal conductance measured vertically. $G_{XY}=G_{YX}$ is a "skew conductance," which vanishes in the presence of mirror symmetry. Given these three parameters, the full four-terminal conductance matrix G_{ij} can be constructed using Eq. (A6).

A second consequence of spin conservation is the quantization of a particular combination of G_{ij}. In particular, in the Appendix we define a third current $I_Z=I_1+I_3$ and a third voltage V_Z which biases lead (2.13) relative to Eq. (2.24). Spin conservation then requires

$$I_Z = G_{ZZ}V_Z, \tag{2.17}$$

with

$$G_{ZZ} = 2\frac{e^2}{h}. \tag{2.18}$$

Since spin nonconserving spin-orbit terms are allowed, spin conservation will not be generically present in the microscopic Hamiltonian of the junction. Nonetheless, we will argue that the low temperature fixed points possess an *emergent* spin conservation, as well as mirror symmetry, so that Eq. (2.18) should hold, albeit with corrections which vanish as a power of temperature.

B. Stable phases

In this section we describe various stable fixed points which admit simple descriptions using bosonization. We will first focus on the limit in which spin is conserved at the junction. There are then four simple fixed points.[15,16] These include the perfectly transmitting (CC) limit, in which both charge and spin conduct, and the perfectly reflecting limit (II), in which both charge and spin are insulating. The mixed fixed points, denoted IC (CI), are perfectly reflecting for charge (spin) and perfectly transmitting for spin (charge).

In the presence of spin nonconserving spin-orbit terms (which preserve time-reversal symmetry) an additional fixed point is possible in which time-reversal symmetry is spontaneously broken. We will see that in the presence of spin-orbit terms this TBI phase is the stable phase when $g<1/2$.

1. Weak backscattering (CC) limit

We first consider the limit where the point contact is nearly open and assume spin is conserved. It will prove useful to follow Ref. 16 and write Eq. (2.13) as a 0+1 dimensional Euclidean path integral for $\theta_{\rho,\sigma}(\tau)\equiv\theta_{\rho,\sigma}(x=0,\tau)$. This formulation is not essential for carrying out the perturbative analysis of this fixed point. However, it is of conceptual value for discussing the duality between different phases, which can be understood in terms of instanton processes in which $\theta_{\rho,\sigma}(\tau)$ tunnels between degenerate minima at strong coupling. This is accomplished by setting up the path integral for $\theta_{\sigma\rho}(x,\tau)$ and then integrating out $\theta_{\sigma,\rho}(x,\tau)$ for $x\neq 0$. The resulting theory for $\theta_{\sigma,\rho}(\tau)$ has the form of a *quantum Brownian motion* model[24,25,28–30] described by the Euclidean action

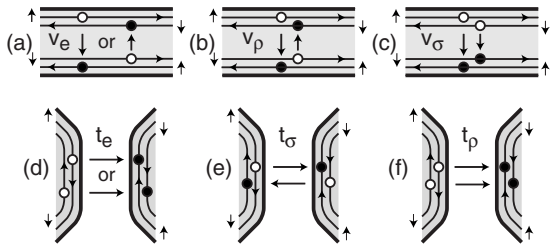

FIG. 2. Schematic representation of tunneling processes in [(a)–(c)] the CC phase (small v) and [(c)–(e)] the II phase (small t). (a) and (d) describe single electron processes, while the others are two particle processes. The duality relating $v_e\leftrightarrow t_e$, $v_\rho\leftrightarrow t_\sigma$, and $v_\sigma\leftrightarrow t_\rho$ can clearly be seen.

$$S_{\rm CC} = \frac{1}{\beta}\sum_{\alpha,\omega_n}\frac{1}{2\pi g_\alpha}|\omega_n||\theta_a(\omega_n)|^2 - \int_0^\beta \frac{d\tau}{\tau_c}V_{\rm CC}(\theta_\sigma,\theta_\rho), \tag{2.19}$$

where $\omega_n=2\pi n/\beta$ are Matsubara frequencies and $\beta=1/k_BT$. We have included the short time cutoff $\tau_c=x_c/v$ in the second term to make the potential $V(\theta_\rho,\theta_\sigma)$ dimensionless. The theory can be regularized by evaluating frequency sums with a $\exp(-|\omega_n|\tau_c)$ convergence factor.

The potential $V(\theta_\rho,\theta_\sigma)$ is given by an expansion in terms of tunneling operators, which represent the processes depicted in Figs. 2(a)–2(c),

$$V_{\rm CC} = v_e\cos(\theta_\rho+\eta_\rho)\cos\,\theta_\sigma + v_\rho\cos 2\theta_\rho + v_\sigma\cos 2\theta_\sigma. \tag{2.20}$$

v_e represents the elementary backscattering of a single electron across the point contact. The phase of $\cos\,\theta_\sigma$ in that term is fixed by time-reversal symmetry. The phase η_ρ of $\cos\,\theta_\rho$ is arbitrary, though mirror symmetry, if present, requires $\eta_\rho=n\pi$. In addition we include compound tunneling processes. v_ρ represents the backscattering of a pair of electrons with opposite spins. We have chosen to define θ_ρ such that the phase of this term is zero. Note that this process involves the tunneling of *spin* (not charge) between the top and bottom edges. Similarly, v_σ represents the transfer of a unit of spin from the right to the left moving channels and involves the tunneling of *charge* $2e$ between the top and bottom edges. In general higher order terms could also be included. However, those terms are less relevant.

The low energy stability of this fixed point is determined by the scaling dimensions $\Delta(v_\alpha)$ of the perturbations, which determine the leading order renormalization group flows,

$$dv_\alpha/d\ell = [1-\Delta(v_\alpha)]v_\alpha. \tag{2.21}$$

These are given by

$$\Delta(v_e) = (g_\rho+g_\sigma)/2 = (g+g^{-1})/2,$$

$$\Delta(v_\rho) = 2g_\rho = 2g,$$

$$\Delta(v_\sigma) = 2g_\sigma = 2g^{-1}. \tag{2.22}$$

It is therefore clear that all operators are irrelevant for $1/2<g<2$, so that the CC phase is stable. For $g<1/2$ v_ρ be-

comes relevant and for $g>2$ v_σ becomes relevant.

At the fixed point the conductance matrix elements are

$$G_{XX} = 2e^2/h,$$

$$G_{YY} = G_{XY} = 0. \tag{2.23}$$

At finite temperature, there will be corrections to these values. The leading corrections will depend on the least irrelevant operators. We find

$$\delta G_{XX} = \begin{cases} -c_1 v_e^2 T^{g+g^{-1}-2}, & g > 1/\sqrt{3} \\ -c_2 v_\rho^2 T^{4g-2}, & g < 1/\sqrt{3}, \end{cases}$$

$$\delta G_{YY} = \begin{cases} c_3 v_e^2 T^{g+g^{-1}-2}, & g < \sqrt{3} \\ c_4 v_\sigma^2 T^{4/g-2}, & g > \sqrt{3}, \end{cases} \tag{2.24}$$

where c_i are nonuniversal constants. Note that for $g<1/\sqrt{3}$ the exponents for G_{XX} and G_{YY} are different. In addition, there will be power-law corrections to G_{XY} when the mirror symmetries $\mathcal{M}_x, \mathcal{M}_y$ are violated. However, this correction is zero when computed from Eqs. (2.19) and (2.20) even when $\eta_\rho \neq 0$ due to the symmetry of Eq. (2.20) under $\theta_\sigma \rightarrow -\theta_\sigma$. Computing G_{XY} requires a higher order irrelevant operator. For instance, $\lambda_1 \partial_x \varphi_\sigma \sin\theta_\rho \cos\theta_\sigma$ and $\lambda_2 \partial_x \varphi_\rho \cos\theta_\rho \sin\theta_\sigma$ break both $\mathcal{M}_X$ and $\mathcal{M}_Y$ while preserving time reversal. This leads to

$$\delta G_{XY} = c_5 \lambda_1 \lambda_2 T^{g+g^{-1}}. \tag{2.25}$$

Note that the temperature exponent of G_{XY} is at least 2 even for weak interactions $g \sim 1$. This is because the tunneling terms λ_1 and λ_2 include an extra derivative term. This is related to the fact (which we will show in Sec. III C) that for noninteracting electrons $G_{XY}=0$. Weak interactions then introduce inelastic processes which give $G_{XY} \propto T^2$. The vanishing of G_{XY} is a unique property of the spin filtered edge states of the QSHI, which does not occur for a generic four-terminal conductance.

2. Weak tunneling (II) limit

When the point contact is pinched off, $\theta_{\rho,\sigma}$ are effectively pinned, and a theory can be developed in terms of electron tunneling process across the point contact. This theory is most conveniently expressed in terms of the *discontinuity* $\tilde{\theta}_{\sigma,\rho} \equiv \varphi^{\text{right}}_{\sigma,\rho} - \varphi^{\text{left}}_{\sigma,\rho}$ across the junction.[31] The theory takes the form

$$S_{\text{II}} = \frac{1}{\beta} \sum_{\alpha,\omega_n} \frac{g_\alpha}{2\pi} |\omega_n| |\tilde{\theta}_a(\omega_n)|^2 - \int_0^\beta \frac{d\tau}{\tau_c} V_{\text{II}}(\tilde{\theta}_\sigma, \tilde{\theta}_\rho), \tag{2.26}$$

with

$$V_{\text{II}} = t_e \cos(\tilde{\theta}_\rho + \eta_\rho) \cos\tilde{\theta}_\sigma + t_\rho \cos 2\tilde{\theta}_\rho + t_\sigma \cos 2\tilde{\theta}_\sigma. \tag{2.27}$$

As depicted in Figs. 2(d)–2(f) t_e represents the tunneling of a single electron from left to right across the junction. t_σ describes the transfer of a unit of spin across the junction. t_ρ describes the tunneling of a pair of electrons with opposite spins.

The relationship between S_{II} and S_{CC} can be understood into two ways. First, since both S_{II} and S_{CC} describe tunneling between the middles of two disconnected Luttinger liquids (either on the top and bottom of the junction or the left and right) the two theories are identical. It is straightforward to see that if we make the identification

$$\theta_\rho \leftrightarrow \tilde{\theta}_\sigma,$$

$$\theta_\sigma \leftrightarrow \tilde{\theta}_\rho, \tag{2.28}$$

it follows that

$$S_{\text{II}}(g_\rho, g_\sigma, t_e, t_\rho, t_\sigma) = S_{\text{CC}}(g_\sigma, g_\rho, v_e, v_\sigma, v_\rho). \tag{2.29}$$

Thus, the small v and small t theories are dual to each other, with the identification

$$v_e \leftrightarrow t_e,$$

$$v_\rho \leftrightarrow t_\sigma,$$

$$v_\sigma \leftrightarrow t_\rho,$$

$$g \leftrightarrow g^{-1}. \tag{2.30}$$

Using this identification, the scaling dimensions $\Delta(t_\alpha)$ can be read off from Eq. (2.22). Thus, like the CC phase, the II phase is stable when $1/2<g<2$. The low temperature conductance can also be read from Eqs. (2.23)–(2.25) using the identification

$$G_{XX} \leftrightarrow G_{YY}. \tag{2.31}$$

Another way to understand this duality, which will prove useful below, is to consider an instanton expansion for strong coupling. For large v_e $(\theta_\rho, \theta_\sigma)$ will be tightly bound at the minima of $V(\theta_\rho, \theta_\sigma)$, shown in Fig. 3(a). (Here we assume for simplicity $\eta_\rho=0$.) The partition function describing the path integral of Eq. (2.19) can then be expanded in instanton processes, in which $(\theta_\rho, \theta_\sigma)$ switches between nearby minima at discrete times. Evaluating the first term in Eq. (2.19) for a configuration of instantons leads to an interaction between the instantons which depends logarithmically on time. The expansion describes the partition function for a one-dimensional "Coulomb gas," where the "charges" correspond to the tunneling events. This Coulomb gas has exactly the same form as the expansion of Eq. (2.26) in powers of t_e, t_ρ, and t_σ. Thus, we can identify t_e, t_ρ, and t_σ as the fugacities of the instantons.

This duality argument also works in reverse. Starting from Eq. (2.26) we can derive Eq. (2.19) by considering large t_e and expanding in instantons in $\tilde{\theta}_\rho$ and $\tilde{\theta}_\sigma$ connecting minima in Fig. 3(b), which have fugacities v_e, v_ρ, and v_σ.

3. Charge insulator/spin conductor (IC)

We next study the mixed charge insulator spin conductor phase. To generate the effective action for this phase, includ-

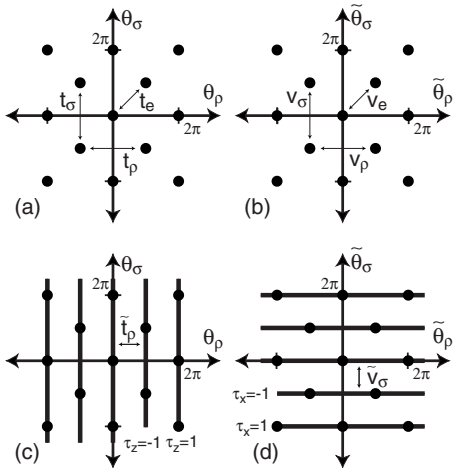

FIG. 3. (a) Positions of the minima of $V(\theta_\rho,\theta_\sigma)$ in Eq. (2.20). When the minima are deep instanton tunneling events between the minima, denoted by t_e, t_ρ, and t_σ, correspond to the transfer of charge and spin across the junction and define the dual theory [Eqs. (2.26) and (2.27)]. (b) Positions of the minima of $V(\tilde{\theta}_\rho,\tilde{\theta}_\sigma)$ in the dual theory [Eqs. (2.26) and (2.27)]. Instanton process v_e, v_ρ, and v_σ correspond to backscattering of charge and spin in the original theory. (c) The IC phase viewed from the CC limit. When v_ρ is large and $v_\sigma=0$, the minima of $V(\theta_\rho,\theta_\sigma)$ in Eq. (2.20) are on one-dimensional valleys and define the IC phase. When v_σ is small but finite the valleys have a periodic potential $\tilde{v}_\sigma\tau^z\cos\theta_\sigma$, with opposite signs $\tau^z=\pm1$ in neighboring valleys. Instanton tunneling processes between the valleys, denoted $\tilde{t}_\rho$, switch the sign of τ^z. (d) The IC phase viewed from the II limit, in which $t_\rho=0$ and t_σ is large. The valleys have periodic potential $\tilde{t}_\rho\tau^x\cos\tilde{\theta}_\rho$ with $\tau^x=\pm1$, whose sign is switched by instanton processes $\tilde{v}_\sigma$.

ing the leading relevant operators, it is useful to use the instanton analysis discussed at the end of Sec. II B 2. Consider Eqs. (2.26) and (2.27) for large v_ρ, keeping v_e and v_σ small. θ_ρ will be pinned in the minima of $-\cos 2\theta_\rho$, $\theta_\rho=n\pi$, while θ_σ remains free to fluctuate. $(\theta_\rho,\theta_\sigma)$ are thus confined to "valleys" along the vertical lines in Fig. 3(c).

There are two types of perturbations to be considered. First, v_e will lead to a periodic potential along the vertical lines, with minima at the dots. Note, however, that on alternate lines the sign of the periodic potential changes since $\cos\theta_\rho\cos\theta_\sigma\sim(-1)^n\cos\theta_\sigma$ for $\theta_\rho=n\pi$.

Next consider an instanton process where θ_ρ tunnels between neighboring valleys. In this process, $\theta_\rho\to\theta_\rho\pm\pi$, but θ_σ is unchanged. It follows that the v_e perturbation discussed above changes sign. Thus, the instanton process does not commute with the v_e term.

The expansion of the partition function in both instantons and v_e can be generated by the action for the IC phase given by $S_{\rm IC}=S^0_{\rm IC}+S^1_{\rm IC}$ with

$$S^0_{\rm IC}=\frac{1}{\beta}\sum_{\omega_n}\frac{g_\rho}{2\pi}|\omega_n||\tilde{\theta}_\rho(\omega_n)|^2+\frac{1}{2\pi g_\sigma}|\omega_n||\theta_\sigma(\omega_n)|^2 \tag{2.32}$$

and

$$S^1_{\rm IC}=\int_0^\beta\frac{d\tau}{\tau_c}[\tilde{t}_\rho\tau^x\cos\tilde{\theta}_\rho+\tilde{v}_\sigma\tau^z\cos\theta_\sigma]. \tag{2.33}$$

Here $\tilde{t}_\rho$ describes the instanton tunneling process. The tilde distinguishes it from the ordinary charge tunneling process, which involves charge $2e$. $\tilde{t}_\rho$ describes a tunneling of charge e *without* spin. $\tilde{v}_\sigma$ describes the periodic potential as a function of θ_σ generated by v_e. We have introduced a pseudospin degree of freedom $\tau^z=\pm1$ to account for the sign of $\cos\theta_\rho$ in the different valleys. Since the instanton process switches the sign, it is associated with τ^x. Expanding the partition function defined by Eqs. (2.32) and (2.33) in powers of $\tilde{t}_\rho$ and $\tilde{v}_\sigma$ precisely generates the expansion of Eqs. (2.19) and (2.20) in instantons.

It is also instructive to derive Eqs. (2.32) and (2.33) starting from the opposite limit of the II phase described by Eqs. (2.26) and (2.27). In this case, consider large t_σ, which leads to the horizontal valleys as a function of $\tilde{\theta}_\rho$ and $\tilde{\theta}_\sigma$ in Fig. 3(d). The roles of the two terms in Eq. (2.33) are thus reversed. $\tilde{t}_\rho$ describes the periodic potential along the valleys, which has a sign specified by $\tau^x=\pm1$. $\tilde{v}_\sigma$ describes the instanton processes which switch the sign of τ^x.

The lowest order renormalization group flows depend only on the scaling dimensions of $\tilde{t}_\rho$ and $\tilde{v}_\sigma$ and are unaffected by the pseudospin $\tau^{x,z}$. We find

$$\Delta(\tilde{t}_\rho)=\frac{1}{2g_\rho}=\frac{1}{2g},$$

$$\Delta(\tilde{v}_\sigma)=\frac{g_\sigma}{2}=\frac{1}{2g}. \tag{2.34}$$

Thus, the IC phase is stable when $g<1/2$.

In Sec. III D we will require the renormalization group flow to third order in $\tilde{t}_\rho$ and $\tilde{v}_\sigma$. There, the nontrivial interaction between them introduced by the pseudospin will play a crucial role.

The conductivity at the IC fixed point is given by

$$G_{XX}=G_{YY}=G_{XY}=0. \tag{2.35}$$

This, however, does *not* mean that the full four-terminal conductance is zero because spin conservation still requires $G_{ZZ}=2e^2/h$. This leads to the nontrivial structure in the four-terminal conductance predicted in Ref. 10.

At finite temperature, there will be corrections to the conductance. We find

$$\delta G_{XX}=d_1\tilde{t}_\rho^2T^{g^{-1}-2},$$

$$\delta G_{YY}=d_2\tilde{v}_\sigma^2T^{g^{-1}-2}. \tag{2.36}$$

As in this section the corrections to G_{XY} will depend on a higher order irrelevant operator. For instance, $\lambda_1\tau^y\sin\tilde{\theta}_\rho\sin\theta_\sigma$ and $\lambda_2\tau^y\cos\tilde{\theta}_\rho\cos\theta_\sigma$ lead to

$$\delta G_{XY} = d_3 \lambda_1 \lambda_2 T^{2g^{-1}-2}. \quad (2.37)$$

As in Eq. (2.25), G_{XY} is suppressed more strongly at low temperature than G_{XX} and G_{YY}, and the exponent is larger than 2 for $g < 1/2$.

4. Charge conductor/spin insulator (CI)

For $g > 2$ the perturbation $v_\sigma \cos 2\theta_\sigma$ in Eq. (2.20) becomes relevant and drives the system to the CI phase. This may be described in a manner similar to the IC phase. It is described by the action $S_{\mathrm{CI}} = S^0_{\mathrm{CI}} + S^1_{\mathrm{CI}}$ with

$$S^0_{\mathrm{CI}} = \frac{1}{\beta}\sum_{\omega_n} \frac{g_\sigma}{2\pi}|\omega_n||\tilde{\theta}_\sigma(\omega_n)|^2 + \frac{1}{2\pi g_\rho}|\omega_n||\theta_\rho(\omega_n)|^2 \quad (2.38)$$

and

$$S^1_{\mathrm{CI}} = \int_0^\beta \frac{d\tau}{\tau_c}[\tilde{t}_\sigma \tau^z \cos(\tilde{\theta}_\sigma + \eta_\sigma) + \tilde{v}_\rho \tau^x \cos(\theta_\rho + \eta_\rho)]. \quad (2.39)$$

The leading relevant operators have dimensions

$$\Delta(\tilde{t}_\sigma) = \frac{1}{2g_\sigma} = \frac{g}{2},$$

$$\Delta(\tilde{v}_\rho) = \frac{g_\rho}{2} = \frac{g}{2}. \quad (2.40)$$

This phase is thus stable when $g > 2$ and has conductances

$$G_{XX} = G_{YY} = 2e^2/h,$$

$$G_{XY} = 0. \quad (2.41)$$

5. Spin-orbit interactions and T-breaking insulator

In this section we consider the role of spin-orbit interaction terms which violate the conservation of spin S_z but respect time-reversal symmetry. We will argue that such terms are irrelevant for the critical behavior of the point contact when $g > 1/2$, but they are relevant for $g < 1/2$ and drive the system at low energy to a TBI.

Time-reversal symmetry allows the following terms in the expansion about CC fixed point (2.19):

$$S^{\mathrm{SO}}_{\mathrm{CC}} = \int_0^\beta \frac{d\tau}{\tau_c}[v_{\mathrm{so}} \cos\varphi_\sigma \sin\theta_\sigma + v_{\mathrm{sf}} \cos(2\varphi_\sigma + \eta_{\mathrm{sf}})]. \quad (2.42)$$

The first term is a single electron process $\psi^\dagger_{R\uparrow}\psi_{R\downarrow}$ [Fig. 4(a)] in which an electron flips its spin and crosses the junction. The second term is a correlated tunneling process $\psi^\dagger_{R\uparrow}\psi^\dagger_{L\uparrow}\psi_{R\downarrow}\psi_{L\downarrow}$ [Fig. 4(b)], where a left and right moving pair of up spins flip into a left and right moving pair of down spins. Referring to Table I, it is clear that both terms respect time-reversal symmetry. η_{sf} is allowed by time-reversal symmetry but violates both mirrors $\mathcal{M}_x$ and $\mathcal{M}_y$. Higher order processes are also possible, though they will be less relevant perturbatively.

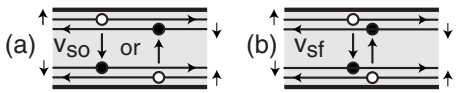

FIG. 4. Tunneling processes in the CC limit allowed by spin nonconserving spin-orbit interactions. v_{so} is a single particle process where a single spin is flipped, while v_{sf} is a two particle process, flipping two spins.

It is straightforward to determine the scaling dimensions of these perturbations. We find

$$\Delta(v_{\mathrm{so}}) = \frac{1}{2}(g_\sigma + g_\sigma^{-1}) = \frac{1}{2}(g + g^{-1}),$$

$$\Delta(v_{\mathrm{sf}}) = \frac{2}{g_\sigma} = 2g. \quad (2.43)$$

For $g \neq 1$ the single particle spin-orbit term v_{so} is always irrelevant. However, v_{sf} becomes relevant when $g < 1/2$.

At finite temperature these lead to corrections to the conductance of the CC phase. To lowest order they do not affect G_{XX}, G_{XY}, and G_{YY}. However we find

$$\delta G_{ZZ} \propto \begin{cases} T^{g+g^{-1}-2}, & g > 1/\sqrt{3} \\ T^{4g-2}, & g < 1/\sqrt{3}. \end{cases} \quad (2.44)$$

Like G_{XY}, G_{ZX} and G_{ZY} are zero unless higher order irrelevant operators, which involve extra powers of $\partial_x\varphi_\alpha$ or $\partial_x\theta_\alpha$, are included. We find

$$\delta G_{ZX} \propto T^{2g},$$

$$\delta G_{ZY} \propto T^{g+g^{-1}}. \quad (2.45)$$

For weak interactions, $g \sim 1$, these conductances vanish for $T \to 0$ as T^2.

For $g < 1/2$ there are two relevant perturbations about the CC limit. To study their effects we consider a model in which only the relevant perturbations appear. Since these perturbations involve the commuting operators φ_σ and θ_ρ, it is useful to study the 0+1 dimensional field theory of those variables,

$$S^0_{\mathrm{CC}} = \sum_{\omega_n} \frac{1}{2\pi g_\rho}|\omega_n||\theta_\rho(\omega_n)|^2 + \frac{g_\sigma}{2\pi}|\omega_n||\varphi_\sigma(\omega_n)|^2, \quad (2.46)$$

with

$$S^1_{\mathrm{CC}} = \int_0^\beta \frac{d\tau}{\tau_c}[v_\rho \cos(2\theta_\rho + \eta_\rho) + v_{\mathrm{sf}} \cos(2\varphi_\sigma + \eta_{\mathrm{sf}})]. \quad (2.47)$$

The low temperature behavior of this theory can be studied by the duality arguments of Sec. II B 2. When v_ρ and v_{sf} are both large, $(\theta_\rho, \varphi_\sigma)$ will be stuck in the deep minima of $V_{\mathrm{CC}}(\theta_\rho, \varphi_\sigma)$ shown in Fig. 5. In this phase, the *four-terminal* conductance is zero,

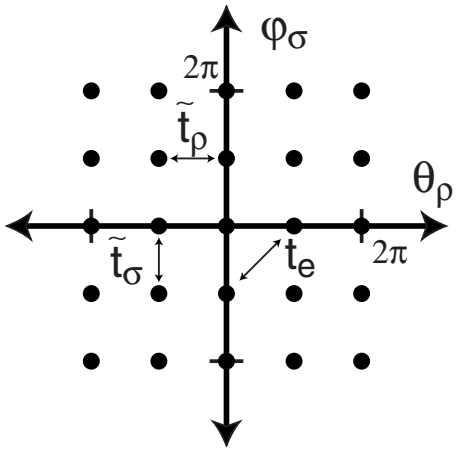

FIG. 5. Minima of the potential $V(\theta_\rho,\varphi_\sigma)$ in Eq. (2.47). Large v_ρ and v_{so} define the time-reversal breaking insulating phase. Instanton processes $\tilde{t}_\rho$ and $\tilde{t}_\sigma$ restore time-reversal invariance. They correspond to tunneling of spinless chargons or chargeless spinons.

$$G_{AB}=0. \tag{2.48}$$

This can be seen most simply by renaming the variables

$$\theta_\rho \to \theta_1+\theta_2,$$

$$\varphi_\sigma \to \theta_1-\theta_2,$$

$$\varphi_\rho \to \varphi_1+\varphi_2,$$

$$\varphi_\sigma \to \varphi_1-\varphi_2. \tag{2.49}$$

The interpretation of $\theta_{1(2)}$ and $\varphi_{1(2)}$ is simple. They are the usual Luttinger liquid charge and phase variables for the top (bottom) edges in Figs. 2(a)–2(c). In the strong coupling phase θ_1 and θ_2 are both pinned, so that any current flowing in from any lead is perfectly reflected back into that lead. The four leads are completely decoupled.

This is the same perfectly reflecting phase that would arise if we had a single particle backscattering term on each edge $v_{\rm back}(\cos 2\theta_1+\cos 2\theta_2)=2v_{\rm back}\cos\theta_\rho\cos\varphi_\sigma$, which would be relevant for $g<1$. However in our problem that term is forbidden by time-reversal symmetry. It is thus clear that time-reversal symmetry is violated by the strong coupling fixed point. It is useful to see this from Fig. 5. Note that since under time reversal $\varphi_\sigma\to\varphi_\sigma+\pi$. Thus pinning φ_σ violates time reversal. There are two sets of minima of $V(\theta_\rho,\varphi_\sigma)$ which are interchanged by the time-reversal operation.

At finite temperature tunneling processes between the two sets of minima of $V(\theta_\rho,\varphi_\sigma)$ will restore time-reversal symmetry. These instanton processes correspond to tunneling of charge from one lead to another. Interestingly, the lowest order instanton processes, denoted $\tilde{t}_\rho$ and $\tilde{t}_\sigma$, *do not* correspond to tunneling of electrons but rather spinless charge e "chargons" or charge neutral "spinons."

The scaling dimensions of these instanton processes can be deduced from Eqs. (2.46) and (2.47). We find

$$\Delta(\tilde{t}_\rho)=\frac{1}{2g_\rho}=\frac{1}{2g},$$

$$\Delta(\tilde{t}_\sigma)=\frac{g_\sigma}{2}=\frac{1}{2g}. \tag{2.50}$$

Thus, both processes are irrelevant for $g<1/2$, and the TBI phase is stable. These processes lead to power-law temperature behavior,

$$\delta G_{XX}=c_1\tilde{t}_\rho^2 T^{1/g-2},$$

$$\delta G_{YY}=c_1\tilde{t}_\sigma^2 T^{1/g-2}. \tag{2.51}$$

When the $\tilde{t}_{\rho,\sigma}$ processes dominate, there will be nontrivial noise correlations in the current. The $\tilde{t}_\rho$ process involves transferring charge $e/2$ from lead 1 to lead 2 and another $e/2$ from lead 4 to lead 3. This leads to correlations in the low frequency noise defined by

$$\mathcal{S}_{ij}(\omega)=\int dt e^{i\omega t}\langle I_i(t)I_j(0)+I_j(0)I_i(t)\rangle. \tag{2.52}$$

Consider the two-terminal geometry $I_X=G_{XX}V_X$. The current I_X will be carried by the $\tilde{t}_\rho$ processes, so that $I_1=I_4=I_X/2$. The shot noise correlations in the limit $\omega\to 0$ will be

$$S_{11}=S_{44}=S_{14}=S_{41}=2e^*I_1 \tag{2.53}$$

with $e^*=e/2$. Thus, the currents are all perfectly correlated, and the current in each lead is carried by *fractional* charges, $e/2$.

III. CRITICAL BEHAVIOR OF CONDUCTANCE

In this section we describe the critical behavior of the conductance at the pinch-off transition of the point contact. We will compute the critical conductance G_g^*, the critical exponent α_g, and the scaling function $\mathcal{G}_g(X)$ in certain solvable limits. We will begin in Sec. III A with a discussion of the general properties of the scaling function and a summary of our calculated results. Then in the following sections we will describe in detail our calculations for $g=1-\epsilon$, $g=1/\sqrt{3}$, and $g=1/2+\epsilon$.

A. Scaling behavior and summary of results

The stability analysis of the previous sections leads to the phase diagram as a function of g depicted in Fig. 6(a). The top line depicts the CC phase and the bottom line depicts the II phase, and the arrows denote the stability associated with the leading relevant operators. Since the II and CC phases are both stable for $1/2<g<2$ they are separated by an intermediate unstable fixed point P, denoted by the dashed central line. For $g<1/2$ the II and CC phases become unstable, and when spin is conserved the flow is toward the IC phase. We will see in Sec. III D that the unstable critical fixed point matches smoothly onto the IC fixed point at $g=1/2$. Similarly, the CI fixed point is stable for $g>2$ and connects to the critical fixed point at $g=2$.

For $1/2<g<2$ the unstable intermediate fixed point P describes the critical behavior of the pinch-off transition of the point contact. We will argue that this fixed point is characterized by a *single* relevant operator, which allows us to

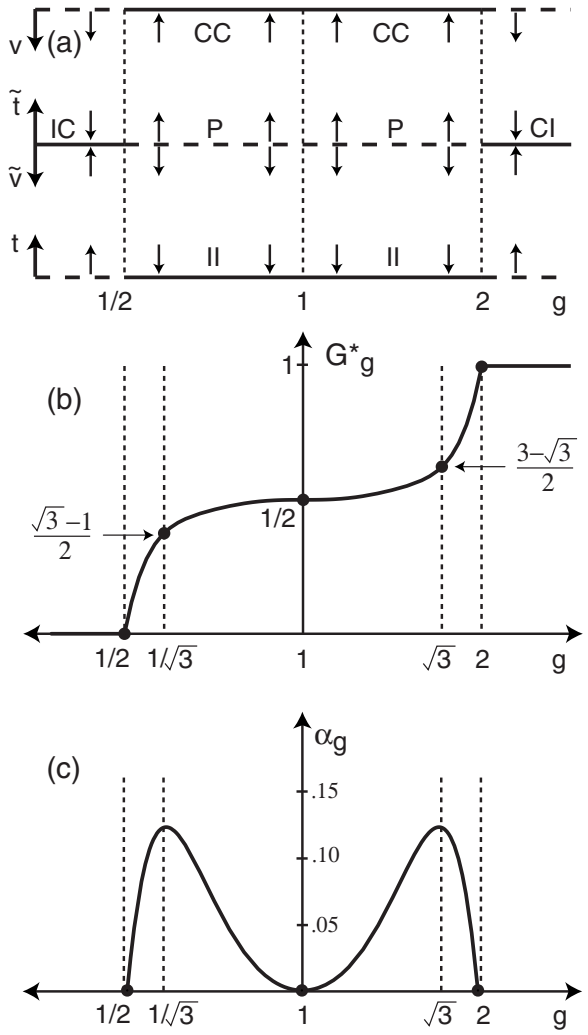

FIG. 6. (a) Phase diagram for a point contact in a QSHI as a function of the Luttinger liquid parameter g. The arrows indicate the stability of the CC, II, CI, and IC phases, as well as the critical fixed point P. This figure assumes spin conservation. In the presence of spin-orbit interactions, the IC phase is unstable for $g<1/2$. This leads to the TBI phase discussed in Sec. II B 5. (b) Conductance G^* of the critical fixed point as a function of g. The curve is a fit, which incorporates the data in Eq. (3.7). (c) Critical exponent α_g as a function of g. The curve is a fit incorporating the data in Eq. (3.8). g is plotted on a logarithmic scale in all three panels to emphasize the $g \leftrightarrow 1/g$ symmetry.

formulate a single parameter scaling theory for the pinch-off transition. If we denote u as the relevant operator, then the leading order renormalization group flow near the fixed point has the form

$$du/d\ell = \alpha_g u, \tag{3.1}$$

where α_g is a critical exponent to be determined. By varying a gate voltage V_G it is possible to cross from the region of stability of the II phase to the region of stability of the CC phase. In the process one must pass through the fixed point $u=0$ at $V_G=V_G^*$. Near the transition, we thus have $u \propto \Delta V_G = V_G - V_G^*$. Under a renormalization group transformation in which energy, length and time are rescaled by b, we have $u \to u b^{\alpha_g}$ and $T \to Tb$. Invariance under this transformation requires that physical quantities can only depend on u and T in the combination u/T^{α_g}. Close to the transition we thus have

$$\lim_{T,\Delta V_G \to 0} G_{AB}(T,\Delta V_G) = 2\frac{e^2}{h}\mathcal{G}_{g,AB}\left(c\frac{\Delta V_G}{T^{\alpha_g}}\right), \tag{3.2}$$

where c is a nonuniversal constant and $\mathcal{G}_{g,AB}$ is a universal crossover scaling function which varies between 0 and 1.

We will argue that the critical point characterizing the pinch-off transition has emergent spin conservation as well as mirror symmetry, so that the only nonzero elements of the conductance matrix are G_{XX} and G_{YY}. Moreover, the duality considerations discussed in Sec. III C require that $\mathcal{G}_{g,YY}(X)$ and $\mathcal{G}_{g,XX}(X)$ are related, so that they are both determined by the same universal scaling function,

$$\mathcal{G}_{g,XX}(X) = \mathcal{G}_g(X),$$

$$\mathcal{G}_{g,YY}(X) = \mathcal{G}_g(-X). \tag{3.3}$$

The scaling function $\mathcal{G}_g(X)$ has some general properties which are easy to deduce. First, the equivalence between the CC theory at g with the II theory at $1/g$ leads to the relation

$$\mathcal{G}_{1/g}(X) = 1 - \mathcal{G}_g(-X). \tag{3.4}$$

Second, when $T \to 0$ for fixed ΔV_G the system flows to either the CC or the II phase, where the temperature dependence of the conductance is given by Eq. (2.24). The behavior of the scaling function for large X then follows

$$\mathcal{G}_g(X \to +\infty) = 1 - a_g^+ X^{-\beta_g^+},$$

$$\mathcal{G}_g(X \to -\infty) = a_g^- X^{-\beta_g^-}. \tag{3.5}$$

The coefficients $a_g^\pm$ depend on the normalization of X but can be fixed if we specify $\mathcal{G}_g'(X=0)=1/2$. The exponents obey the relations

$$\beta_g^+ = \begin{cases} (4g-2)/\alpha_g, & 1/2 < g < 1/\sqrt{3} \\ (g+g^{-1}-2)/\alpha_g, & 1/\sqrt{3} < g < 1, \end{cases}$$

$$\beta_g^- = (g+g^{-1}-2)/\alpha_g \quad 1/2 < g < 1. \tag{3.6}$$

The behavior of $\beta_g^\pm$ for $1<g<2$ can be deduced using Eq. (3.4).

In the following sections we compute properties of the scaling function at $g=1-\epsilon$, $g=1/\sqrt{3}$, and $g=1/2+\epsilon$. From Eq. (3.4) we can deduce corresponding results at $g=1+\epsilon$, $g=\sqrt{3}$, and $g=2-\epsilon$. First consider the critical conductance $G_g^*=\mathcal{G}_g(X=0)$. We find

$$G_g^* = \begin{cases} 1/2 + O(\epsilon^3), & g = 1-\epsilon \\ (\sqrt{3}-1)/2, & g = 1/\sqrt{3} \\ \pi^2\epsilon, & g = 1/2+\epsilon. \end{cases} \tag{3.7}$$

These results are summarized in Fig. 6(b). The curve is a polynomial fit of $G^*(\ln g)$ which incorporates the data in Eq. (3.7) and the $g \leftrightarrow 1/g$ symmetry. It is satisfying that the

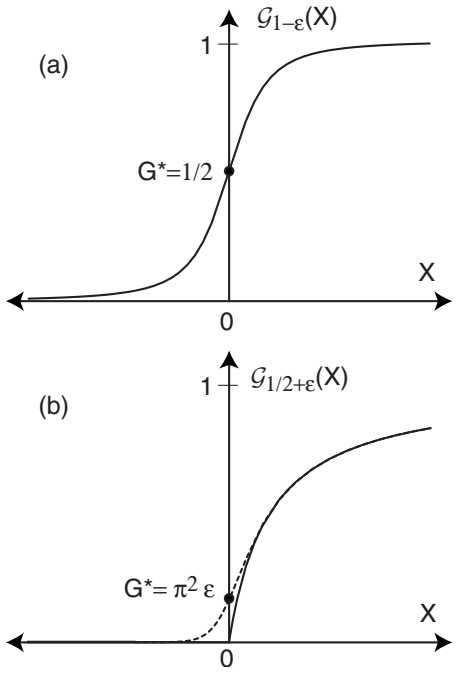

FIG. 7. The universal scaling function $\mathcal{G}_g(X)$ for (a) $g=1-\epsilon$ [Eq. (3.9)] and (b) $g=1/2+\epsilon$ [Eq. (3.10)]. In (b) the solid line is $\epsilon \to 0$, and the dashed line shows the approximate behavior for $\epsilon \sim .02$.

curve is smooth and monotonic, which indicates a consistency between the slopes at $g=1/2,1$ and the value at $g=1/\sqrt{3}$.

We are able to deduce the critical exponent α_g for $g=1-\epsilon$ and $g=1/2+\epsilon$. We find

$$\alpha_g = \begin{cases} \epsilon^2/2, & g = 1-\epsilon \\ 4\epsilon, & g = 1/2+\epsilon. \end{cases} \tag{3.8}$$

These results are summarized in Fig. 6(c). The curve is a polynomial fit of $\alpha(\ln g)$. It is suggestive that in this fit α_g exhibits a maximum near $g=1/\sqrt{3}$ with a value $\alpha_{1/\sqrt{3}}=0.123\sim 1/8$. It is possible, however, that α_g exhibits a cusp at $g=1/\sqrt{3}$ analogous to the behavior of β_g in Eq. (3.6).

In Secs. III C and III D we compute the full scaling function $\mathcal{G}_g(X)$ in the limits $g=1-\epsilon$ and $g=1/2+\epsilon$ to lowest order in ϵ. For $g=1+\epsilon$, $\epsilon \to 0$ we find

$$\mathcal{G}_1(X) = \frac{1}{2}\left(1 + \frac{X}{\sqrt{1+X^2}}\right). \tag{3.9}$$

For $g=1/2+\epsilon$, $\epsilon \to 0$,

$$\mathcal{G}_{1/2}(X) = \theta(X)\frac{X}{1+X}. \tag{3.10}$$

The singular behavior near $X=0$ in Eq. (3.10) is rounded for finite ϵ. The perturbative analysis in Sec. III D 1 shows that for $|X| \ll 1$

$$\mathcal{G}_{1/2+\epsilon}(X) = \frac{X}{1-e^{-X/(\pi^2\epsilon)}}. \tag{3.11}$$

$\mathcal{G}_{1-\epsilon}(X)$ and $\mathcal{G}_{1/2+\epsilon}(X)$ are plotted in Figs. 7(a) and 7(b). For g close to 1 the pinch-off curve is symmetrical about $G^*=e^2/h$. However, for stronger repulsive interactions it becomes asymmetrical, as G^* is reduced, approaching 0 at $g=1/2$.

TABLE II. Parameters in Eq. (3.5) for the asymptotic behavior of the scaling function $\mathcal{G}_g(X)$ in the solvable limits $g \to 1$, $g \to 1/2$.

g	β_g^+	a_g^+	β_g^-	a_g^-
$1-\epsilon$	2	1/4	2	1/4
$1/2+\epsilon$	1	1	$1/(8\epsilon)$	$(2.75)^{1/(8\epsilon)}$

The asymptotic $|X| \to \infty$ behavior (3.5) of $\mathcal{G}_1(X)$ and $\mathcal{G}_{1/2+\epsilon}$ can also be determined from Eqs. (3.9) and (3.10) though a separate calculation (see Sec. III D 3) is required for $\mathcal{G}_{1/2+\epsilon}(X \to -\infty)$. The results, which are consistent with Eq. (3.6), are shown in Table II.

B. Quantum Brownian motion model, duality, and $g=1/\sqrt{3}$

In this section we recast the Luttinger liquid model as a model of QBM in a periodic potential. This mapping elucidates the duality between the CC and II limits and exposes an extra symmetry, the problem at $g=1/\sqrt{3}$, which allows us to deduce the critical conductance at that point. We begin with a brief review of the QBM model and then derive its consequences for the scaling functions $\mathcal{G}_g(X)$ and $G^*_{1/\sqrt{3}}$.

1. Quantum Brownian motion model

The QBM model[28–30] was originally formulated as a theory of the motion of a heavy particle coupled to an Ohmic dissipative environment modeled as a set of Caldeira-Leggett oscillators.[32] Though the applicability of this model to the motion of a real particle coupled to phonons or electron-hole pairs has been questioned,[33,34] it was later shown that this model is directly relevant to quantum impurity problems. Specifically, the QBM model in a one-dimensional periodic potential is equivalent to the theory of a weak link in a single-channel Luttinger liquid.[16,18] In this mapping the QBM takes place in an abstract space where the "coordinate" of the "particle" is the number of electrons that have tunneled past the weak link. The periodic potential is due to the discreteness of the electron's charge. The low energy excitations of the Luttinger liquid play the role of the dissipative bath, and the strength of the dissipation is related to the Luttinger liquid parameter g. The one-dimensional QBM model has two phases: a localized phase with conductance $G=0$ stable for $g<1$ and a fully coherent phase with perfect conductance stable for $g>1$.

The SLL model corresponds to a QBM model in a two-dimensional periodic potential, where the coordinates are the spin and charge variables $\theta_{\rho,\sigma}$. This model is richer than its one-dimensional counterpart because it admits additional fixed points which are intermediate between localized and perfect. These fixed points were first found in the Luttinger liquid model[15,16] and later formulated in terms of the QBM.[25] For certain values of g_ρ and g_σ these intermediate fixed points are related to the three-channel Kondo problem[25] and the three state Potts models.[24] However, those limits are not

directly applicable to the QSHI model, where $g_\rho = 1/g_\sigma = g$. We will show that when $g = 1/\sqrt{3}$ the critical fixed point of the QSHI point contact corresponds to the intermediate point discussed in Ref. 25 for a QBM model on a triangular lattice.

To formulate the QBM model we begin with action (2.19) and define new rescaled variables,

$$\theta_\alpha = \pi\sqrt{2g_\alpha}r_\alpha. \tag{3.12}$$

Then Eq. (2.19) takes the form

$$S = \frac{1}{4\pi\beta}\sum_n |\omega_n||\mathbf{r}(\omega_n)|^2 - \int \frac{d\tau}{\tau_c}\sum_{\mathbf{G}} v_{\mathbf{G}} e^{2\pi i \mathbf{G}\cdot\mathbf{r}(\tau)}. \tag{3.13}$$

The periodic potential is characterized by reciprocal lattice vectors $\mathbf{G} = m_1\mathbf{b}_1 + m_2\mathbf{b}_2$. The primitive reciprocal lattice vectors $\mathbf{b}_{1,2}$ correspond to the single electron back scattering processes and are given by

$$\mathbf{b}_1 = \frac{1}{\sqrt{2}}(\sqrt{g_\rho}, \sqrt{g_\sigma}), \quad \mathbf{b}_2 = \frac{1}{\sqrt{2}}(\sqrt{g_\rho}, -\sqrt{g_\sigma}). \tag{3.14}$$

The Fourier components of the periodic potential are $v_{\mathbf{b}_1} = v_{\mathbf{b}_2} = v_e e^{i\eta_\rho}/4$, $v_{\mathbf{b}_1+\mathbf{b}_2} = v_\rho/2$, and $v_{\mathbf{b}_1-\mathbf{b}_2} = v_\sigma/2$.

The dual theory is obtained by expanding the partition function for large $v_{\mathbf{G}}$ in powers of instantons. When $v_{\mathbf{G}}$ is large, the potential has minima on a real space lattice $\mathbf{R} = n_1\mathbf{a}_1 + n_2\mathbf{a}_2$. The primitive lattice vectors satisfy $\mathbf{a}_i \cdot \mathbf{b}_j = \delta_{ij}$ and are given by

$$\mathbf{a}_1 = \frac{1}{\sqrt{2}}\left(\frac{1}{\sqrt{g_\rho}}, \frac{1}{\sqrt{g_\sigma}}\right), \quad \mathbf{a}_2 = \frac{1}{\sqrt{2}}\left(\frac{1}{\sqrt{g_\rho}}, -\frac{1}{\sqrt{g_\sigma}}\right). \tag{3.15}$$

The expansion in instantons connecting these minima is generated by the action

$$S = \frac{1}{4\pi\beta}\sum_n |\omega_n||\mathbf{k}(\omega_n)|^2 - \sum_{\mathbf{R}} \int \frac{d\tau}{\tau_c} t_{\mathbf{R}} e^{2\pi i \mathbf{R}\cdot\mathbf{k}(\tau)}. \tag{3.16}$$

This is equivalent to Eqs. (2.26) and (2.27) with $k_\alpha = \pi\sqrt{g_\alpha/2}\tilde{\theta}_\alpha$ and $t_{\mathbf{a}_1} = t_{\mathbf{a}_2} = t_e e^{i\eta_\rho}/4$, $t_{\mathbf{a}_1+\mathbf{a}_2} = t_\rho/2$, and $t_{\mathbf{a}_1-\mathbf{a}_2} = t_\sigma/2$.

With the above normalizations for $\mathbf{r}$ and $\mathbf{k}$ the scaling dimensions of the potential perturbations are

$$\Delta(v_{\mathbf{G}}) = |\mathbf{G}|^2, \quad \Delta(t_{\mathbf{R}}) = |\mathbf{R}|^2. \tag{3.17}$$

Since operators are relevant when $\Delta < 1$, the most relevant potentials are those with the smallest lattice (reciprocal lattice) vectors $|\mathbf{R}_{\min}|$ ($|\mathbf{G}_{\min}|$). As shown in Refs. 16 and 25 there are ranges of g_ρ and g_σ where both $|\mathbf{R}_{\min}|$ and $|\mathbf{G}_{\min}| > 1$, so that both phases are perturbatively stable. An unstable intermediate fixed point must therefore be present between them.

This fixed point can be accessed perturbatively when $|\mathbf{R}_{\min}|$ and $|\mathbf{G}_{\min}|$ are close to 1. While this does not occur in the regime $g_\rho = 1/g_\sigma$ relevant to the QSHI problem, it is instructive to study this perturbation theory because it provides evidence that the critical fixed point has emergent mirror and spin conservation symmetry.

When $g_\rho = 1/2 + \epsilon_\rho$ and $g_\sigma = 3/2 + \epsilon_\sigma$ the period potential has triangular symmetry, which is slightly distorted if $\epsilon_\sigma \neq 3\epsilon_\rho$. If we denote the relevant variables as $v_1 = v_{\mathbf{b}_1} = v_{\mathbf{b}_2} = v_e e^{i\eta_\rho}/4$ and $v_2 = v_{\mathbf{b}_1+\mathbf{b}_2} = v_\rho/2$, the second-order renormalization group flow equations are[16]

$$dv_1/d\ell = \frac{1}{2}(\epsilon_\rho + \epsilon_\sigma)v_1 - 2v_1^* v_2,$$

$$dv_2/d\ell = 2\epsilon_\rho v_2 - 2v_1^2. \tag{3.18}$$

These equations describe an intermediate fixed point with a single unstable direction at $v_1 = \sqrt{\epsilon_\rho(\epsilon_\rho+\epsilon_\sigma)}/2$ and $v_2 = (\epsilon_\rho + \epsilon_\sigma)/4$. Note that at the critical point v_1 is *real*, so that $\eta_\rho = 0$. Thus the critical point has an emergent mirror symmetry even if the bare parameters in the model do not. Moreover, the flow out of the fixed point along the single unstable direction is also along a line with v_1 real. Thus the crossover between the intermediate fixed point and the trivial fixed point, which determines the crossover scaling function, also has emergent mirror symmetry. Mirror symmetry breaking is an irrelevant perturbation at the critical fixed point.

If $\epsilon_\sigma = 3\epsilon_\rho$ then the lattice vectors have a triangular symmetry. In this case, the fixed point is at $v_1 = v_2 = \epsilon_\rho$. This means that the periodic potential at the fixed point has emergent *triangular symmetry* even when the bare potential does not. The unstable flow out of the fixed point is also along the high symmetry line $v_1 = v_2$.

It seems quite likely that the critical fixed point and unstable flows connecting it to the trivial fixed points retain their high symmetry even outside the perturbative small ϵ regime. This suggests that in general the critical fixed point has mirror symmetry and that at $g = 1/\sqrt{3}$ it has triangular symmetry. We will use this fact below to determine the critical conductance at $g = 1/\sqrt{3}$.

2. Kubo conductance, mobility, and duality relations

The spin and charge conductances in the Luttinger liquid model computed by the Kubo formula are given by a retarded current-current correlation function. For the present discussion it is useful to write this as an imaginary time correlation function, which can be analytically continued to real time via $i\omega \to \omega + i\eta$ before taking the $\omega \to 0$ limit. Then

$$G^K_{\alpha\beta}(i\omega_n) = \frac{1}{\hbar|\omega_n|}\int d\tau e^{i\omega_n\tau}\langle J_\alpha(\tau)J_\beta(0)\rangle, \tag{3.19}$$

where the spin and charge currents are $J_\alpha = e\partial_t\theta_\alpha/\pi = e[\theta, \mathcal{H}]/(i\pi\hbar)$. This may be expressed as

$$G^K_{\alpha\beta}(\omega_n) = 2\frac{e^2}{h}\sqrt{g_\alpha g_\beta}\mu_{\alpha\beta}(\omega_n), \tag{3.20}$$

where the *mobility* of the QBM model is

$$\mu_{\alpha\beta}(\omega_n) = 2\pi|\omega_n|\langle r_\alpha(-\omega_n)r_\beta(\omega_n)\rangle. \tag{3.21}$$

$\mu_{\alpha\beta}$ is normalized so that when $v_{\mathbf{G}} = 0$ $\mu_{\alpha\beta} = \delta_{\alpha\beta}$.

The conductance or equivalently $\mu_{\alpha\beta}$ can also be computed from the dual model. It is given by

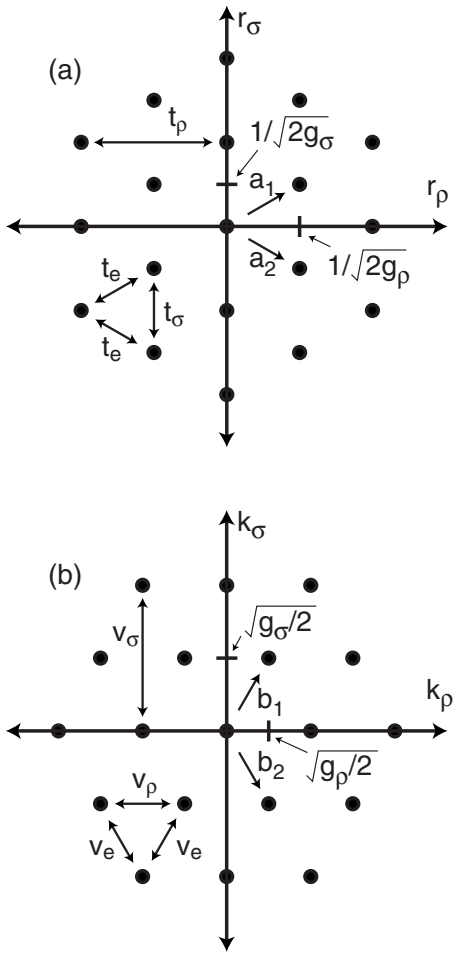

FIG. 8. (a) Minima of the periodic potential $V(\mathbf{r})$ in Eq. (3.13). (b) Minima of $V(\mathbf{k})$ in dual theory (3.16). When $g_\sigma=3g_\rho$ both periodic potentials have triangular symmetry at the critical point, which implies that the mobility $\mu^*_{\alpha\beta}$ is isotropic. This occurs at $g=1/\sqrt{3}$.

$$\mu_{\alpha\beta} = \delta_{\alpha\beta} - \tilde{\mu}_{\alpha\beta}, \tag{3.22}$$

where the *dual* mobility is

$$\tilde{\mu}_{\alpha\beta}(\omega_n) = 2\pi|\omega_n|\langle k_\alpha(-\omega_n)k_\beta(\omega_n)\rangle. \tag{3.23}$$

Equations (3.22) and (3.23) are obvious in the perfectly transmitting and perfectly reflecting limits. They can be derived more generally by starting with a Hamiltonian formulation of the action, analogous to Eq. (2.13), which involves both $\mathbf{r}$ and $\mathbf{k}$. $\mu_{\alpha\beta}$ can then be computed either by first integrating out $\mathbf{k}$ to obtain Eq. (3.21) or first integrating out $\mathbf{r}$ to obtain Eq. (3.23).

Since $g_\rho=1/g_\sigma=g$, the dual theory depicted in Fig. 8(b) is identical to the original theory shown in Fig. 8(a) with the identification $r_\rho \leftrightarrow k_\sigma$, $r_\sigma \leftrightarrow k_\rho$. It follows that the mobility $\mu^*_{\alpha\beta}$ of the fixed point satisfies

$$\mu^*_{\alpha\beta} = [\sigma^x \tilde{\mu}^* \sigma^x]_{\alpha\beta}. \tag{3.24}$$

In addition, if u parametrizes the relevant direction at the critical fixed point, then under the duality $u \to -u$. It follows that slightly away from the critical fixed point we have

$$\mu_{\alpha\beta}(u) = [\sigma^x \tilde{\mu}(-u)\sigma^x]_{\alpha\beta}. \tag{3.25}$$

Properties (3.22) and (3.25) imply that $\mu_{\rho\rho}(u)=1-\mu_{\sigma\sigma}(-u)$. Using Eqs. (3.2), (3.20), and (A15), this leads directly to property (3.3) of the crossover scaling function.

An additional set of relations follows from the equivalence between the theory characterized by g and the dual theory characterized by $1/g$. From this we conclude that

$$\mu_{g,\alpha\beta}(u) = \tilde{\mu}_{1/g,\alpha\beta}(u). \tag{3.26}$$

This, combined with Eqs. (3.2), (3.20), (3.22), and (A15) leads to Eq. (3.4).

3. Conductance at $g=1/\sqrt{3}$

When $g=1/\sqrt{3}$ the lattice generated by $\mathbf{b}_1$ and $\mathbf{b}_2$ has triangular symmetry. In Sec. III B 1 we argued that this means that at the critical fixed point the periodic potential also has triangular symmetry. The C_6 rotational symmetry of the triangular lattice requires that the mobility is *isotropic*,

$$\mu_{\alpha\beta} = \mu_0 \delta_{\alpha\beta}. \tag{3.27}$$

Combining Eqs. (3.22), (3.24), and (3.27) requires that

$$\mu_0 = \frac{1}{2}. \tag{3.28}$$

It follows from Eq. (3.20) that the Kubo formula spin and charge conductances are given by

$$G^K_{\rho\rho} = \sqrt{3}\frac{e^2}{h}, \quad G^K_{\sigma\sigma} = \frac{1}{\sqrt{3}}\frac{e^2}{h}. \tag{3.29}$$

It is well known that the physical conductance measured with leads is not given by the Kubo conductance.[35–39] Rather, the Kubo conductance needs to be modified to account for the contact resistance between the Luttinger liquid and the leads. In the Appendix we review the relation between the physical four-terminal conductance and the Kubo conductance. From Eq. (A19) we conclude that

$$G_{XX} = G_{YY} = (\sqrt{3}-1)\frac{e^2}{h}. \tag{3.30}$$

C. Weak interactions: $g=1-\epsilon$

In this section we develop a perturbative expansion for weak interactions to compute exactly the crossover scaling function $\mathcal{G}_g(X)$ as well as the critical exponent α_g for $g=1-\epsilon$. A similar approach was employed by Matveev *et al.*[27] to compute the scaling function for the crossover between the weak barrier and strong barrier limits in a single-channel Luttinger liquid. In the single-channel problem the transmission for noninteracting electrons is characterized by a transmission probability $\mathcal{T}$. Weak forward scattering interactions lead to an exchange correction to $\mathcal{T}$ at first order in the interactions. This correction diverges for $E \to E_F$ as $\ln|E-E_F|$. Matveev *et al.*[27] used a renormalization group argument to sum the logarithmic divergent corrections to all orders to obtain the exact transmission $\mathcal{T}(E)$.

For noninteracting electrons, the QSHI point contact is characterized by a 4×4 scattering matrix S_{ij} which relates the incoming wave in lead i to the outgoing wave in lead j,

$$|\psi_{i,\text{out}}\rangle = S_{ij}|\psi_{j,\text{in}}\rangle. \tag{3.31}$$

In terms of S_{ij} the four-terminal conductance is

$$G_{ij} = \frac{e^2}{h}(\delta_{ij} - |S_{ij}|^2). \tag{3.32}$$

Under time reversal $\Theta|\psi_{i,\text{out(in)}}\rangle = +(-)Q_{ij}|\psi_{j,\text{in(out)}}\rangle$, where $Q=\text{diag}(1,-1,1,-1)$. This leads to the constraint $S=-QS^TQ$. This combined with unitarity $S^\dagger S=1$ allows S to be parametrized as

$$S = U^\dagger \begin{pmatrix} 0 & t & f & r \\ t & 0 & r^* & -f^* \\ -f & r^* & 0 & -t^* \\ r & f^* & -t^* & 0 \end{pmatrix} U, \tag{3.33}$$

where $U_{ij}=\delta_{ij}e^{i\chi_i}$ is an unimportant gauge transformation. The complex numbers t and r describe the amplitudes for spin conserving transmission and reflection across the point contact, while f describes the amplitude for tunneling across the junction, combined with a spin flip. $f=0$ if spin is conserved. The conductance can be expressed in terms of the transmission probabilities $\mathcal{R}=|r|^2$, $\mathcal{T}=|t|^2$, and $\mathcal{F}=|f|^2$, which satisfy $\mathcal{R}+\mathcal{T}+\mathcal{F}=1$. We find

$$G_{XX} = \frac{2e^2}{h}(\mathcal{T}+\mathcal{F}),$$

$$G_{YY} = \frac{2e^2}{h}(\mathcal{R}+\mathcal{F}),$$

$$G_{ZZ} = \frac{2e^2}{h}(1-\mathcal{F}),$$

$$G_{AB} = 0 \quad \text{for } A \neq B. \tag{3.34}$$

For a generic four-terminal conductance device time-reversal symmetry guarantees only the reciprocity relation[40] $G_{ij}=G_{ji}$ (or equivalently $G_{AB}=G_{BA}$). For the QSHI point contact, the spin filtered nature of the edge states leads to additional constraints. First, the amplitude for an electron to be reflected back into the lead it came from is $S_{ii}=0$. Thus $G_{ii}=e^2/h$. A second less obvious constraint is that $G_{13}=G_{24}$, which when combined with reciprocity and unitarity is equivalent to $G_{12}=G_{34}$ and $G_{14}=G_{23}$. This leads to the vanishing of the skew conductance G_{XY}, as well as G_{XZ} and G_{YZ} even when mirror symmetries $\mathcal{M}_X$ and $\mathcal{M}_Y$ are explicitly violated. This is a property of the noninteracting electron model and can be violated with electron electron interactions if the mirror symmetries are absent.

In order to compute the renormalization of the S matrix due to interactions it is useful to study the perturbative expansion of the single electron thermal Green's function, which can be represented as a matrix in the lead indices i, j as well as the channel labels $a=\text{in/out}$. Here,

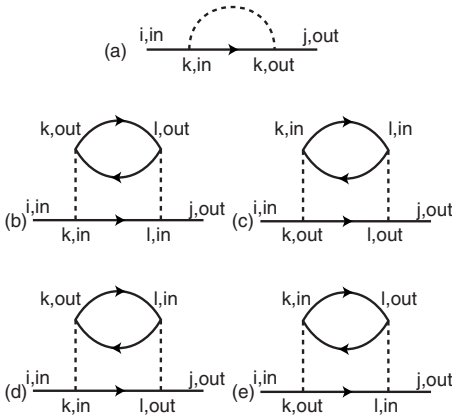

FIG. 9. Feynman diagrams for the single electron Green's function. The dashed line is the interaction $u_2(\psi^\dagger_{\text{in}}\psi_{\text{in}})(\psi^\dagger_{\text{out}}\psi_{\text{out}})$. The exchange diagram (a) vanishes because it involves S_{kk} and diagrams (b) and (c) cancel one another. (d) and (e) lead to a logarithmic correction to the S matrix given in Eq. (3.38).

$$\mathbb{G}^{ab}_{ij}(x,\tau;x',\tau') = -i\langle T_\tau[\psi_{i,a}(x,\tau)\psi^\dagger_{j,b}(x',\tau')]\rangle, \tag{3.35}$$

where T_τ denotes imaginary time ordering. For noninteracting electrons we have

$$\mathbb{G}_{ij}(z,z') = \frac{1}{2\pi i}\begin{pmatrix} \dfrac{\delta_{ij}}{z-z'} & \dfrac{S^*_{ji}}{z-\bar{z}'} \\ \dfrac{S_{ij}}{\bar{z}-z'} & \dfrac{\delta_{ij}}{\bar{z}-\bar{z}'} \end{pmatrix}, \tag{3.36}$$

where $z=\tau+ix$ and $\bar{z}=\tau-ix$, and the $a=\text{in/out}$ indices are displayed in matrix form.

We now compute the perturbative corrections to $\mathbb{G}^{\text{out,in}}_{ij}$ using the standard diagrammatic technique. For simplicity, we adopt a model in which $u_4=0$, so that the only interaction term involves $u_2(\psi^\dagger_{\text{in}}\psi_{\text{in}})(\psi^\dagger_{\text{out}}\psi_{\text{out}})$. This considerably simplifies the analysis because many of the diagrams are zero. For instance, the exchange diagram shown in Fig. 9(a), which was responsible for the renormalization in the single-channel Luttinger liquid problem, is zero because it must involve $\mathbb{G}^{\text{in,out}}_{kk}$. This off-diagonal Green's function depends on S_{kk} which is zero due to the time-reversal-symmetry constraint. From Eq. (2.9), $g=\sqrt{(2\pi v_F-\lambda_2)/(2\pi v_F+\lambda_2)}\sim 1-\lambda_2/(2\pi v_F)$. Thus for $g=1-\epsilon$ we may replace u_2 by $2\pi v_F\epsilon$. The nonzero diagrams at second order in u_2 are shown in Figs. 9(b)–9(e). Evaluating the second-order diagrams gives a Green's function of the form

$$\mathbb{G}^{\text{out,in}}_{ij} = \frac{1}{2\pi i}\frac{S'_{ij}}{\bar{z}-z'} \tag{3.37}$$

with

$$S'_{ij} = S_{ij} + \frac{\epsilon^2}{4}\ln\frac{\Lambda}{E}\left[S_{ij}S_{ji}S^*_{ji} - \sum_{kl} S_{ik}S_{kl}S^*_{lk}S^*_{kl}S_{lj}\right], \tag{3.38}$$

where Λ are E are ultraviolet and infrared cutoffs, respectively. The first term in the brackets was due to the diagram

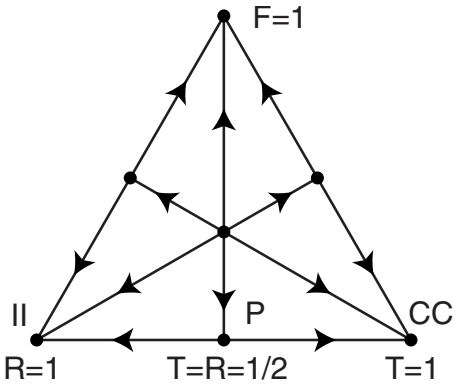

FIG. 10. Renormalization group flow diagram for the transmission probabilities $\mathcal{T}$, $\mathcal{R}$, and $\mathcal{F}$ based on Eq. (3.40) represented in a ternary plot. The CC, II, and P fixed points of interest in this paper, which have $\mathcal{F}=0$ are on the bottom of the triangle.

in Fig. 9(d), while the second term was from Fig. 9(e). Diagrams in Figs. 9(b) and 9(c) canceled each other. Rescaling the cutoff $\Lambda \to \Lambda e^{-\ell}$ leads to a renormalization group flow equation for S_{ij},

$$\frac{dS_{ij}}{d\ell} = \frac{\epsilon^2}{4}\left[S_{ij}S_{ji}S^*_{ji} - \sum_{kl} S_{ik}S_{kl}S^*_{lk}S^*_{kl}S_{lj} \right]. \tag{3.39}$$

It is useful to rewrite this in terms of the transmission probabilities $\mathcal{T}$, $\mathcal{R}$, $\mathcal{F}$. The renormalization group flow equation then can be written in the form

$$d\mathcal{T}/d\ell = \epsilon^2 \mathcal{T}(\mathcal{T} - \mathcal{T}^2 - \mathcal{R}^2 - \mathcal{F}^2),$$

$$d\mathcal{R}/d\ell = \epsilon^2 \mathcal{R}(\mathcal{R} - \mathcal{T}^2 - \mathcal{R}^2 - \mathcal{F}^2),$$

$$d\mathcal{F}/d\ell = \epsilon^2 \mathcal{F}(\mathcal{F} - \mathcal{T}^2 - \mathcal{R}^2 - \mathcal{F}^2). \tag{3.40}$$

The flow diagram as a function of $\mathcal{R}$, $\mathcal{T}$, and $\mathcal{F}$ is shown in Fig. 10. There are seven fixed points. The bottom corners of the triangle are the stable fixed points at $\mathcal{R}=1$, $\mathcal{T}=\mathcal{F}=0$ (the II phase) and $\mathcal{T}=1$, $\mathcal{R}=\mathcal{F}=0$ (the CC phase). The third stable fixed point at the top of the triangle with $\mathcal{F}=1$, $\mathcal{T}=\mathcal{R}=0$ corresponds to the case where an incident electron is transmitted perfectly with a spin flip. This is presumably difficult to access physically. On the edges of the triangle are unstable fixed points describing transitions between the different stable phases. The critical fixed point P of interest in this paper is the one on the bottom of the triangle at $\mathcal{R}=\mathcal{T}=1/2$, $\mathcal{F}=0$. Note that at this fixed point the spin nonconserving spin-orbit processes, represented by $\mathcal{F}$, are irrelevant. At the center of the triangle, at $\mathcal{R}=\mathcal{T}=\mathcal{F}=1/3$ is an unstable fixed point describing a multicritical point.

To describe the critical fixed point P and the crossover to the II and CC phases we now specialize to $\mathcal{F}=0$ and consider the flow equation for the single parameter $\mathcal{T}$ characterizing the point contact

$$d\mathcal{T}/d\ell = -\epsilon^2 \mathcal{T}(1-\mathcal{T})(1-2\mathcal{T}). \tag{3.41}$$

Equation (3.41) can be integrated to determine the crossover scaling function. If at $\ell=0$, $\mathcal{T}=\mathcal{T}^0$, then,

$$\mathcal{T}(\ell) = \frac{1}{2}\left[1 + \frac{\mathcal{T}^0 - 1/2}{\sqrt{(\mathcal{T}^0 - 1/2)^2 + \mathcal{T}^0(1-\mathcal{T}^0)e^{-\epsilon^2\ell}}} \right]. \tag{3.42}$$

As the gate voltage V_G is adjusted through the pinch-off transition, $\mathcal{T}^0$ passes through 1/2 at $V_G = V_G^*$, so $\mathcal{T}^0 - 1/2 \propto \Delta V_G$. At temperature T we cut off the renormalization group flow at $\Lambda e^{-\ell} \propto T$. The conductance is then given by $G_{XX} = 2(e^2/h)\mathcal{T}[\ell = \ln(\Lambda/T)]$. For $\Delta V_G, T \to 0$ we define $X = (2\mathcal{T}^0 - 1)e^{\epsilon^2 \ell/2} \propto \Delta V_G / T^{\epsilon^2/2}$ and write the conductance in the scaling form,

$$G_{XX}(\Delta V_G, T) = 2\frac{e^2}{h}\mathcal{G}_{1-\epsilon}\left(c\frac{\Delta V_G}{T^{\alpha_g}} \right), \tag{3.43}$$

where c is a nonuniversal constant, the critical exponent is

$$\alpha_{1-\epsilon} = \epsilon^2/2, \tag{3.44}$$

and

$$\mathcal{G}_{1-\epsilon}(X) = \frac{1}{2}\left[1 + \frac{X}{\sqrt{1+X^2}} \right]. \tag{3.45}$$

We find that the logarithmic renormalization to the S matrix accounts for the *only* correction to the conductance to linear order in ϵ. In principle one must consider a "random-phase-approximation-type" diagram for the conductance evaluated by the Kubo formula. While this gives a correction for an *infinite* Luttinger liquid at finite frequency, the correction is zero for a finite Luttinger liquid connected to leads in the $\omega \to 0$ limit.[35–38] Since the critical conductance satisfies $G_g^* = 1 - G_{1/g}^*$ it follows that $G_{1-\epsilon}^* = 1/2 + O(\epsilon^3)$.

D. $g = 1/2 + \epsilon$

$g=1/2$ is at the boundary where the CC and II phases become unstable and the IC phase becomes stable. We will show that when $g=1/2+\epsilon$ the critical fixed point describing the transition between the CC and II phases approaches the IC fixed point and can be accessed perturbatively using theory developed in Sec. II B 3. In addition, when $g=1/2$, the marginal operators $v_\rho \cos 2\theta_\rho$ at the CC fixed point and $\tilde{t}\cos\tilde{\theta}_\rho$ at the IC fixed point can be expressed in terms of fictitious fermion operators. This fermionization process allows the entire crossover between the CC and IC phases to be described using a noninteracting fermion Hamiltonian. A similar fermionization procedure can be used to describe the crossover between the II and IC phases, which connect the marginal operators $\tilde{v}_\sigma \cos\theta_\sigma$ and $\tilde{t}_\sigma \cos 2\tilde{\theta}_\sigma$. This will allow us to compute the full crossover scaling function $\mathcal{G}_g(X)$ for $g=1/2+\epsilon$.

We will begin by discussing the perturbative analysis of the IC fixed point and then go on to describe the fermionization procedure.

1. Perturbative analysis

The IC fixed point is described by Eqs. (2.32) and (2.33). When $g=1/2+\epsilon$ the perturbations $\tilde{t}_\rho \tau^x \cos\tilde{\theta}_\rho$ and $\tilde{t}_\sigma \tau^z \cos\theta_\sigma$

both have scaling dimension $\Delta=1-2\epsilon$, so the IC fixed point is weakly unstable. When $\tilde{v}_\sigma=0$, nonzero $\tilde{t}_\rho$ is expected to drive the system to the CC phase, while for $\tilde{t}_\rho=0$ nonzero $\tilde{v}_\sigma$ will drive the system to the II phase. Thus, when both $\tilde{t}_\rho$ and $\tilde{v}_\sigma$ are nonzero there must be an unstable fixed point which separates the two alternatives. This fixed point can be described by considering the renormalization group flow equations to *third* order in $\tilde{v}_\sigma$ and $\tilde{t}_\rho$.

The first-order renormalization group equation for $\tilde{t}_\rho$ is determined by the scaling dimension $\Delta(\tilde{t}_\rho)$. The next nonzero term occurs at order $t_\rho v_\sigma^2$. To compute this term it is sufficient to use the theory at $\epsilon=0$. Consider the third-order term in the cumulant expansion of the partition function when fast degrees of freedom integrated out,

$$\frac{1}{2}\int d\tau_1 d\tau_2 \{\langle T_\tau[O_\rho(\tau)O_\sigma(\tau_1)O_\sigma(\tau_2)]\rangle_> - \langle O_\rho(\tau)\rangle_>\langle T_\tau[O_\sigma(\tau_1)O_\sigma(\tau_2)]\rangle_>\}. \quad (3.46)$$

Here $O_\rho=(\tilde{t}_\rho/\tau_c)\tau^x\cos\tilde{\theta}_\rho$ and $O_\sigma=(\tilde{v}_\sigma/\tau_c)\tau^z\cos\theta_\sigma$. T_τ indicates time ordering, and $\langle\cdot\rangle_>$ denotes a trace over degrees of freedom with $\Lambda/b<\omega<\Lambda$, and we assume for simplicity $b\gg 1$. Since $\tilde{\theta}_\rho$ and θ_σ are independent and commute with one another the other disconnected terms all cancel. Moreover, the two terms in Eq. (3.46) will cancel each other unless the time ordering of the τ^x and τ^z operators leads to a relative minus sign between them,

$$\langle T_\tau[O_\rho(\tau)O_\sigma(\tau_1)O_\sigma(\tau_2)]\rangle_> = s_\pm\langle O_\rho(\tau)\rangle_>\langle T_\tau[O_\sigma(\tau_1)O_\sigma(\tau_2)]\rangle_>, \quad (3.47)$$

where $s_\pm=\mathrm{sgn}(\tau-\tau_1)(\tau-\tau_2)$. Thus the pseudospin operators in Eq. (2.33) play a crucial role in the renormalization of $\tilde{t}_\rho$. Using the fact that $\langle T_\tau[O_\sigma(\tau_1)O_\sigma(\tau_2)]\rangle_>=\tilde{v}_\sigma^2/2(\tau_1-\tau_2)^2$ for $\epsilon=0$ we find that the third-order correction to $\tilde{t}_\rho$ is $\delta\tilde{t}_\rho=-t_\rho v_\sigma^2\ln b$. This leads to the renormalization group flow equation for $\tilde{t}_\rho$ along with a corresponding equation for $\tilde{v}_\sigma$,

$$d\tilde{t}_\rho/d\ell = 2\epsilon\tilde{t}_\rho - \tilde{t}_\rho\tilde{v}_\sigma^2,$$

$$d\tilde{v}_\sigma/d\ell = 2\epsilon\tilde{v}_\sigma - \tilde{v}_\sigma\tilde{t}_\rho^2. \quad (3.48)$$

The renormalization group flow diagram is shown in Fig. 11. There is an unstable fixed point P at $\tilde{t}_\rho=\tilde{v}_\sigma=\sqrt{2\epsilon}$, with a single relevant operator. P separates the flows to the CC and II phases for which $\tilde{t}_\rho$ or $\tilde{v}_\sigma$ grows. Note that spin-orbit terms such as v_{so} and v_{sf} discussed in Sec. II B 5 are irrelevant at P [see Eq. (2.43)]. This perturbative calculation provides further evidence that P exhibits emergent spin conservation, as well as emergent mirror symmetry. The critical exponent associate with the single relevant operator P is

$$\alpha_{1/2+\epsilon}=4\epsilon. \quad (3.49)$$

The Kubo conductance $G^K_{\rho\rho}$ at the fixed point can be computed from Eq. (3.19) by identifying the current operator

$$I_\rho=(\tilde{t}_\rho/\tau_c)\sin\tilde{\theta}_\rho. \quad (3.50)$$

This leads to

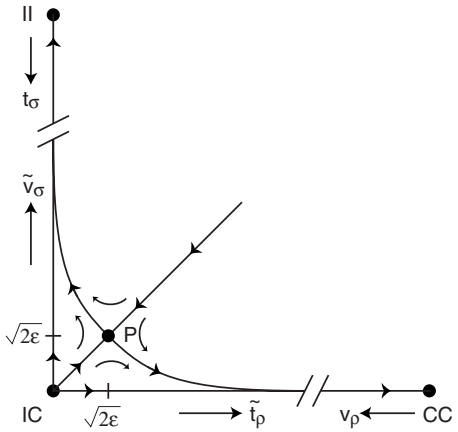

FIG. 11. Renormalization group flow diagram characterizing the critical fixed point P for $g=1/2+\epsilon$. When $\tilde{v}_\sigma$ and $\tilde{t}_\rho$ are small, the flows are given by Eq. (3.48). On the axis $\tilde{v}_\sigma=0$ the fermionization procedure outlined in Sec. III D 2 determines the entire crossover between the IC and CC fixed points. A similar theory describes the crossover between the IC and II fixed points for $\tilde{t}_\rho=0$.

$$G^K_{\rho\rho}=\frac{e^2}{h}\pi^2\tilde{t}_\rho^2. \quad (3.51)$$

It is useful to define $\mathcal{T}_\rho=\pi^2\tilde{t}_\rho^2$. We will see in Sec. III D 2 that this can be interpreted as a transmission probability for fictitious free fermions that describe the problem at $g=1/2$. In terms of $\mathcal{T}_\rho$ (noting that $\mathcal{T}_\rho\ll 1$ in this perturbative regime) we may use Eq. (A19) to write the physical conductance as

$$G_{XX}=\frac{e^2}{h}\mathcal{T}_\rho. \quad (3.52)$$

A similar calculation gives

$$G_{YY}=\frac{e^2}{h}\mathcal{R}_\sigma, \quad (3.53)$$

where $\mathcal{R}_\sigma=\pi^2\tilde{v}_\sigma^2$ can similarly be interpreted as a reflection probability for a different fictitious free fermion at $g=1/2$. At the critical fixed point $\mathcal{T}_\rho=\mathcal{R}_\sigma=2\pi^2\epsilon$. Thus,

$$G^*_{XX}=G^*_{YY}=2\frac{e^2}{h}\pi^2\epsilon,$$

$$G^*_{XY}=0. \quad (3.54)$$

The behavior away from the critical point can be determined by integrating Eq. (3.48). To this end it is helpful to rewrite Eq. (3.48) in terms of $\mathcal{T}_\rho$ and $\mathcal{R}_\sigma$ in the following forms:

$$d(\mathcal{T}_\rho-\mathcal{R}_\sigma)/d\ell=4\epsilon(\mathcal{T}_\rho-\mathcal{R}_\sigma),$$

$$d\ln(\mathcal{T}_\rho/\mathcal{R}_\sigma)/d\ell=(2/\pi^2)(\mathcal{T}_\rho-\mathcal{R}_\sigma). \quad (3.55)$$

If $(\mathcal{T}_\rho,\mathcal{R}_\sigma)=(\mathcal{T}_\rho^0,\mathcal{R}_\sigma^0)$ for $\ell=0$, then we find

$$\mathcal{T}_\rho(\ell) = \frac{(\mathcal{T}_\rho^0 - \mathcal{R}_\sigma^0)e^{4\epsilon\ell}}{1 - \frac{\mathcal{R}_\sigma^0}{\mathcal{T}_\rho^0}\exp\left[-\frac{\mathcal{T}_\rho^0 - \mathcal{R}_\sigma^0}{2\pi^2\epsilon}(e^{4\epsilon\ell}-1)\right]},$$

$$\mathcal{R}_\sigma(\ell) = \frac{(\mathcal{R}_\sigma^0 - \mathcal{T}_\rho^0)e^{4\epsilon\ell}}{1 - \frac{\mathcal{T}_\rho^0}{\mathcal{R}_\sigma^0}\exp\left[-\frac{\mathcal{R}_\sigma^0 - \mathcal{T}_\rho^0}{2\pi^2\epsilon}(e^{4\epsilon\ell}-1)\right]}. \quad (3.56)$$

At the pinch-off transition $V_G = V_G^*$, $\mathcal{R}_0 = \mathcal{T}_0$. Thus, $\mathcal{T}_0 - \mathcal{R}_0 \propto \Delta V_G$. At temperature T we cut off the renormalization group flow at $\Lambda e^{-\ell} \propto T$. Thus, in the limit $\Delta V_G, T \to 0$ we define $X = (\mathcal{T}_\rho^0 - \mathcal{R}_\sigma^0)e^{4\epsilon\ell}/2 \propto \Delta V_G / T^{4\epsilon}$. The conductance then has the form

$$G_{XX}(\Delta V_G, T) = 2\frac{e^2}{h}\mathcal{G}_g\left(c\frac{\Delta V_G}{T^{\alpha_g}}\right),$$

$$G_{YY}(\Delta V_G, T) = 2\frac{e^2}{h}\mathcal{G}_g\left(-c\frac{\Delta V_G}{T^{\alpha_g}}\right), \quad (3.57)$$

with

$$\mathcal{G}_{1/2+\epsilon}(X) = \frac{X}{1 - e^{-X/(\pi^2\epsilon)}}. \quad (3.58)$$

This perturbative calculation is only valid when $\mathcal{T}_\rho, \mathcal{R}_\sigma \ll 1$. Thus Eq. (3.58) breaks down at low temperature since as the energy is lowered either $\mathcal{T}_\rho$ or $\mathcal{R}_\sigma$ grows. Equation (3.58) is valid as long as $|X| \ll 1$. Note, however, that when $\epsilon \ll 1$ we have $\mathcal{G}_{1/2+\epsilon}(X) = X\theta(X)$ when $\epsilon \ll X \ll 1$. In this regime, the smaller of $\mathcal{T}$ and $\mathcal{R}$ has gone to zero. Thus we have

$$\left.\begin{aligned}\mathcal{T}_\rho(\ell) &= (\mathcal{T}_\rho^0 - \mathcal{R}_\sigma^0)e^{4\epsilon\ell}\\ \mathcal{R}_\sigma(\ell) &= 0\end{aligned}\right\}(\mathcal{T}_\rho^0 - \mathcal{R}_\sigma^0) > 0,$$

$$\left.\begin{aligned}\mathcal{T}_\rho(\ell) &= 0\\ \mathcal{R}_\sigma(\ell) &= (\mathcal{R}_\sigma^0 - \mathcal{T}_\rho^0)e^{4\epsilon\ell}\end{aligned}\right\}(\mathcal{R}_\sigma^0 - \mathcal{T}_\rho^0) > 0, \quad (3.59)$$

and the unstable flow is either on the x or y axis of Fig. 11. In Sec. III D 2 we will solve the crossover exactly on these lines. This will allow us to compute the $\mathcal{G}_{1/2+\epsilon}(X)$ exactly for all X.

2. Fermionization

In this section we study the crossover between the IC fixed point and the CC and II fixed points for $g = 1/2 + \epsilon$. There are two cases to consider. First, for $\Delta V_G > 0$ we will study the crossover between the IC and CC on the horizontal axis of Fig. 11 with $\tilde{v}_\sigma = 0$. This problem can be mapped to a single-channel one-dimensional Fermi gas with weak electron-electron interactions proportional to ϵ. This allows us to use the method of Matveev *et al.*[27] to compute the crossover scaling functions $\mathcal{G}_{g,XX}(X)$ and $\mathcal{G}_{g,YY}(X)$ for $X > 0$ exactly. For $\Delta V_G < 0$ the crossover between the IC and II fixed points is on the vertical axis of Fig. 11 with $\tilde{t}_\rho = 0$. This can be fermionized by introducing a *different* set of free fermions to compute the scaling functions for $X < 0$. The latter calculation (which is virtually identical to the former) is unnecessary, however, because we can use Eq. (3.3) to deduce the scaling functions for $X < 0$. We will therefore focus on the IC to CC crossover.

The crossover between the IC and the CC fixed points can be described by the action in the CC limit,

$$S_{\mathrm{CC}} = \frac{1}{\beta}\sum_n \frac{1}{2\pi g}|\omega_n||\theta_\rho(\omega_n)|^2 + \int d\tau v_\rho \cos 2\theta_\rho. \quad (3.60)$$

$v_\rho \ll 1$ describes the CC phase. When $v_\rho \gg 1$ the dual theory, formulated as in Sec. II B 3 in terms of instantons with amplitude $\tilde{t}_\rho$, describes the IC phase. When $\tilde{v}_\sigma = 0$ at the IC fixed point we can safely ignore the pseudospin and set $\tau^x = 1$.

For $g = 1/2$ this model is equivalent to the bosonized representation of a weak link in a single-channel *noninteracting* fermion with weak backscattering. Here,

$$\mathcal{H}_f = -iv\tilde{\psi}^\dagger\partial_x\sigma^z\tilde{\psi} + v_f\tilde{\psi}^\dagger\sigma^x\tilde{\psi}\delta(x), \quad (3.61)$$

where $\tilde{\psi} = (\tilde{\psi}_R, \tilde{\psi}_L)^T$ is a two component fermion operator describing right and left movers. Using bosonization relation (2.3) we identify $2\theta_\rho = \phi_R - \phi_L$ and $v_f = \pi v_\rho / v$. The free fermion problem is solvable and characterized by a transmission probability $\mathcal{T}_\rho = \mathrm{sech}^2(v_f/v)$. The free fermion solution therefore connects the CC limit ($\mathcal{T}_\rho = 1$) with the IC limit ($\mathcal{T}_\rho = 0$).

The Kubo conductance $G_{\rho\rho}^K$ may be computed with the identification $J_\rho = \partial_t\theta_\rho/\pi = v\tilde{\psi}^\dagger\sigma^z\tilde{\psi}$, giving

$$G_{\rho\rho}^K = \frac{e^2}{h}\mathcal{T}_\rho. \quad (3.62)$$

Note that this is the same as Eq. (3.52), derived in the opposite limit near the IC fixed point. When v_ρ is large, $\mathcal{T}_\rho \ll 1$, and we can identify $\mathcal{T}_\rho = (\pi\tilde{t}_\rho)^2$. The physical conductance, measured with leads, can be determined following the analysis in the Appendix. From Eq. (A19) we find

$$G_{XX} = 2\frac{e^2}{h}\frac{\mathcal{T}_\rho}{2 - \mathcal{T}_\rho}. \quad (3.63)$$

Since $v_\sigma = 0$ in Eq. (3.60), we have

$$G_{YY} = 0. \quad (3.64)$$

For $g = 1/2 + \epsilon$ the IC fixed point becomes slightly unstable, while the CC fixed point becomes slightly stable. In this case the free fermion problem includes a weak *attractive* interaction

$$\mathcal{H}_f^{\mathrm{int}} = -u_f(\tilde{\psi}_L^\dagger\tilde{\psi}_L)(\tilde{\psi}_R^\dagger\tilde{\psi}_R), \quad (3.65)$$

with $u_f = 2\pi v\epsilon$. This leads to a logarithmic renormalization of $\mathcal{T}_\rho$, which drives a crossover to the CC limit. The correction to $\mathcal{T}_\rho$ occurs at *first* order in u_f and is due to the exchange diagram, shown in Fig. 9(a). The analysis is exactly the same as that performed by Matveev *et al.* As in Sec. III C the result can be cast in terms of a renormalization group flow equation for $\mathcal{T}_\rho$,

$$d\mathcal{T}_\rho/d\ell = 4\epsilon\mathcal{T}_\rho(1-\mathcal{T}_\rho). \tag{3.66}$$

Integrating Eq. (3.66) gives

$$\mathcal{T}_\rho(\ell) = \frac{\mathcal{T}_\rho^0 e^{4\epsilon\ell}}{1+\mathcal{T}_\rho^0(e^{4\epsilon\ell}-1)}, \tag{3.67}$$

where $\mathcal{T}_\rho^0=\mathcal{T}_\rho(\ell=0)$. The scaling function for $\Delta V_G>0$ then follows by using the initial condition from Eq. (3.59), so that $\mathcal{T}_\rho^0 \propto \Delta V_G$. Then, for $\Delta V_G, T\to 0$ we define $X=\mathcal{T}_\rho^0 e^{4\epsilon\ell}/2 \propto \Delta V_G/T^{4\epsilon}$. Using Eqs. (3.63), (3.64), and (3.67), the conductance has the scaling form for $X>0$,

$$\mathcal{G}_{XX,1/2+\epsilon}(X) = \frac{X}{X+1},$$

$$\mathcal{G}_{YY,1/2+\epsilon}(X) = 0. \tag{3.68}$$

Using Eq. (3.3), we may deduce the corresponding behavior for $\Delta V_G<0$ (or $X<0$). The scaling function then has the form

$$\mathcal{G}_{1/2+\epsilon}(X) = \theta(X)\frac{X}{X+1}. \tag{3.69}$$

Note that for $X\ll 1$, $\mathcal{G}_{1/2+\epsilon}(X)=X\theta(X)$, in agreement with the limiting behavior of Eq. (3.58) for $X\gg\epsilon$. These two expressions can thus be combined to give

$$\mathcal{G}_{1/2+\epsilon}(X) = \frac{X}{X+1-e^{-X/(\pi^2\epsilon)}}, \tag{3.70}$$

which reproduces Eq. (3.58) when $|X|\sim\epsilon\ll 1$ and Eq. (3.69) when $|X|\gg\epsilon$. This function is plotted in Fig. 7(b). Note, however, that this formula does not correctly capture the leading behavior for $X<0$ when $|X|\gg\epsilon$. In particular, it misses the $X\to-\infty$ behavior, which Eqs. (3.5) and (3.6) predict is proportional to $|X|^{-1/(8\epsilon)}$. This regime is analyzed in Sec. III D 3.

3. Rebosonization

We now analyze the leading behavior of $\mathcal{G}_{1/2+\epsilon}(X)$ for $X<0$ and $|X|\gg\epsilon$ when ϵ is small. Equivalently, we consider $\mathcal{G}_{1/2+\epsilon,YY}(X)$ for $X>0$. This requires extending the renormalization group flow equation for $\tilde{v}_\sigma$ given in Eq. (3.48) to all $\tilde{t}_\rho$ (or equivalently $\mathcal{T}_\rho$). This can be done by using the fermionized representation of $\tilde{t}_\rho\tau^x\cos\tilde{\theta}_\rho$ in Eq. (2.33). The key point is that the presence of the pseudospin operator τ^x means that the operator $\tilde{v}_\sigma\tau^z\cos\theta_\sigma$ changes the sign of the transmission amplitude for the fermions $\tilde{\psi}$. This results in an x-ray edge-like contribution to the renormalization of $\tilde{v}_\sigma$. This can be computed by a method analogous to that used by Schotte and Schotte[41] to solve the x-ray edge problem, which involves transforming the noninteracting fermions to even and odd parity scattering states and then rebosonizing. This approach was used to study the x-ray edge problem in a Luttinger liquid in Ref. 42.

We begin by writing Eq. (2.33), $\mathcal{H}=\mathcal{H}_\sigma+\mathcal{H}_\rho$, with

$$\mathcal{H}_\sigma = \mathcal{H}_\sigma^0 + \tilde{v}_\sigma\tau^z\cos\theta_\sigma \tag{3.71}$$

and

$$\mathcal{H}_\rho = -iv\tilde{\psi}^\dagger\sigma^z\partial_x\tilde{\psi} + t_f\tau^x\tilde{\psi}^\dagger\sigma^x\tilde{\psi}\delta(x). \tag{3.72}$$

Here $\mathcal{H}_\sigma^0$ is the σ part of Eq. (2.13), and we explicitly account for the pseudospin τ^x. Equation (3.72) can be rebosonized by first replacing $\psi_2(x)\to\psi_2(-x)$, which transforms the nonchiral fermions to chiral fermions, eliminating the σ^z in the first term but leaving the second term alone. Then we perform a SU(2) rotation $(\tilde{\psi}_1,\tilde{\psi}_2)\to(\tilde{\psi}_e,\tilde{\psi}_o)$, which changes σ^x in the second term into σ^z. $\tilde{\psi}_{e(o)}$ describe the even (odd) parity scattering states characterized by scattering phase shifts $\delta_e=-\delta_o$ that specify $\tilde{\psi}_{e(o)}(x>0)=e^{2i\delta_{e(o)}}\tilde{\psi}_{e(o)}(x<0)$. We next bosonize $\tilde{\psi}_{e,o}\to e^{i\phi_{e,o}}/\sqrt{2\pi x_c}$ and define $\phi_\pm=\phi_e\pm\phi_o$. Then

$$\mathcal{H}_\rho = \frac{v}{8\pi}[(\partial_x\phi_+)^2+(\partial_x\phi_-)^2] + \frac{v}{2\pi}\delta_-\tau^x(\partial_x\phi_-)\delta(x), \tag{3.73}$$

where $\phi_\pm$ obey, $[\phi_\pm(x),\phi_\pm(x')]=2\pi i\,\mathrm{sgn}(x-x')$. $\delta_-=\delta_e-\delta_o$ is related to the transmission probability by

$$\mathcal{T}_\rho = \sin^2\delta_-. \tag{3.74}$$

δ_- can be eliminated from Eq. (3.73) by the canonical transformation $U=\exp[i\tau^x\delta_-\phi_-(x=0)/(2\pi)]$, which shifts $\phi_-\to\phi_-+\mathrm{sgn}(x)\delta_-\tau^x$. This transformation also rotates τ^z in Eq. (3.71), which becomes

$$\mathcal{H}_\sigma = H_\sigma^0 + \tilde{v}_\sigma[\tau^+e^{i\phi_-\delta_-/\pi}+\tau^-e^{-i\phi_-\delta_-/\pi}]\cos\theta_\sigma, \tag{3.75}$$

where $\tau^\pm=\tau^z\pm i\tau^y$. The renormalization of $\tilde{v}_\sigma$ can then easily be determined for arbitrary δ_-. We find

$$\frac{d\tilde{v}_\sigma}{d\ell} = \left(2\epsilon-\left(\frac{\delta_-}{\pi}\right)^2\right)\tilde{v}_\sigma. \tag{3.76}$$

For small $\tilde{t}_\rho$, $\delta_-=\pi\tilde{t}_\rho$, and Eq. (3.76) reproduces Eq. (3.48). However, Eq. (3.76) remains valid to lowest order in ϵ for all $\mathcal{T}_\rho$.

We now integrate Eq. (3.55) to a scale ℓ_0 where from Eq. (3.56) $\mathcal{T}_\rho(\ell_0)=2X_0$ and $\mathcal{R}_\sigma(\ell_0)=2X_0e^{-X_0/(\pi^2\epsilon)}$ are small. [Here $X_0=(\mathcal{T}_\rho^0-\mathcal{R}_\sigma^0)e^{4\epsilon\ell_0}/2$.] We then use that as an initial value for Eq. (3.76), which we integrate assuming $\mathcal{T}_\rho(\ell)$ is given by Eq. (3.67) and is unaffected by the small $\mathcal{R}_\sigma$. Expressing Eq. (3.67) in terms of Eq. (3.74) we have

$$\delta_-(\ell) = \tan^{-1}[\delta_-(\ell_0)e^{2\epsilon(\ell-\ell_0)}], \tag{3.77}$$

where $\delta_-(\ell_0)=\sin^{-1}\sqrt{\mathcal{T}_\rho(\ell_0)}\sim\sqrt{2X_0}$. As before, we define $X=(\mathcal{T}_\rho^0-\mathcal{R}_\sigma^0)e^{4\epsilon\ell}/2$. We may express $G_{YY}=(e^2/h)\mathcal{R}_\sigma$ with $\mathcal{R}_\sigma=\pi^2\tilde{v}_\sigma^2$. Integrating Eq. (3.76) we then find

$$G_{YY}(X) = 2\frac{e^2}{h}Xe^{-F(X)/\epsilon}, \tag{3.78}$$

where

$$F(X) = \frac{1}{\pi^2}\int_0^{\sqrt{2X}}\frac{dx}{x}(\tan^{-1}x)^2. \tag{3.79}$$

Thus, for $X<0$, $|X|\gg\epsilon$, and $\epsilon\to 0$ we find

$$\mathcal{G}_{1/2+\epsilon}(X) = |X|e^{-F(|X|)/\epsilon}. \tag{3.80}$$

The asymptotic behavior $F(X)=X/\pi^2$ for $|X|\ll 1$ reproduces Eq. (3.58) when $|X|\gg\epsilon$. For $|X|\gg 1$ we find

$$F(X\to\infty) = \frac{1}{8}\ln 2X - \frac{7\zeta(3)}{4\pi^2}, \tag{3.81}$$

where $\zeta(3)=1.20$ is the Riemann zeta function. This gives the asymptotic behavior

$$\mathcal{G}_{1/2+\epsilon}(X\to-\infty) = \left(\frac{e^{14\zeta(3)/\pi^2}}{2|X|}\right)^{1/8\epsilon}, \tag{3.82}$$

which is quoted in Table II.

IV. DISCUSSION AND CONCLUSION

In this paper we have examined several properties of a point contact in a QSHI. We showed that the pinch-off as a function of gate voltage is governed by a nontrivial quantum phase transition, which leads to scaling behavior of the conductance as a function of temperature and gate voltage characterized by a universal scaling function. We computed this scaling function and other properties of the critical point in certain solvable limits which provide an overall picture of the behavior as a function of the Luttinger liquid parameter g.

In addition, we showed that the four-terminal conductance has a simple structure when expressed in terms of the natural variables, G_{AB}, and that at the low temperature fixed points, the leading corrections to the different components of G_{AB} can have different temperature dependences. In particular, we showed that the skew conductance G_{XY} vanishes as T^γ with $\gamma\geq 2$.

Finally, we showed that for strong interactions, $g<1/2$, the stable phase is the time-reversal breaking insulating phase. Transport in that phase occurs via novel fractionalized excitations that have clear signatures in noise correlations.

There are a number of problems for future research that our work raises. We will divide the discussion into experimental and theoretical issues.

A. Experimental issues

The QSHI has been observed in transport experiments on HgTe/HgCdTe quantum well structures. A crucial issue is the value of the interaction parameter g. A simple estimate can be developed based on the long range Coulomb interaction.[43] First consider the limit $\xi\gg w$, where w is the quantum well width and ξ is the evanescent decay length of the edge state wave function into the bulk QSHI. We model the edge state as a two-dimensional charged sheet with a charge density profile proportional to $\theta(x)\exp(-2x/\xi)$, a distance d above a conducting ground plane. The long range interaction then leads to $u_2=u_4=(2e^2/\epsilon)\ln(4e^\gamma d/\xi)$, where ϵ is the dielectric constant and $\gamma=0.577$ is Euler's constant. As a second model, assume $\xi\ll w$ and model the edge state as a uniformly charged two-dimensional strip of width w perpendicular to a ground plane a distance d away. This gives $u_2=u_4=(2e^2/\epsilon)\ln(2e^{3/2}d/w)$. The intermediate regime $\xi\sim w$ can be solved numerically, and we find that it is accurately described by a simple interpolation between the above limits with $4d/(\xi e^{-\gamma}+2we^{-3/2})$ in the logarithm. This leads to[44]

$$g = \left[1+\frac{2}{\pi}\frac{e^2}{\epsilon\hbar v_F}\ln\left(\frac{7.1d}{\xi+0.8w}\right)\right]^{-1/2}. \tag{4.1}$$

For $\epsilon=15$, $\hbar v_F=.35$ eV nm, $\xi=2\hbar v_F/E_{\rm gap}\sim 30$ nm ($E_{\rm gap}$ is the gap of the bulk QSHI), $w=12$ nm, and $d=150$ nm (Ref. 45) this predicts $g\sim 0.8$. The critical exponent governing the temperature dependence of pinch-off curve (1.1) is then $\alpha_g\sim 0.02$. In the CC and II phases the conductance vanishes as T^δ with $\delta_g=g+g^{-1}-2\sim 0.05$.

The good news is that since g is close to 1 the low temperature scaling behavior should be accurately described by scaling function (3.9) computed in the limit $g\to 1$. The bad news is that the smallness of α_g and δ_g means that it will be difficult to see much dynamic range in the conductance as a function of temperature. Nonetheless, it may be possible to observe logarithmic corrections to the conductance as a function of temperature, and by comparing pinch-off curves at different temperatures it may be possible to observe the predicted sharpening of the transition as temperature is lowered.

The skew conductance G_{XY} is predicted be zero for noninteracting electrons and with weak interactions vanishes as T^2. This is a consequence of the unique edge state structure of the QSHI and remains robust when the interactions are weak.

To probe the critical behavior of the pinch-off transition, as well as the more exotic strong interaction phases it would be desirable to engineer structures with smaller g. Perhaps this could be accomplished by modifying either the dielectric environment or the bare Fermi velocity of the edge states. Maciejko *et al.*[12] suggested that this may be possible using InAs/GaSb/AlSb type-II quantum wells.[46,47]

B. Theoretical issues

Our work points to a number of theoretical problems for future study. It would be very interesting if the powerful framework of conformal field theory can be used to analyze the intermediate critical fixed point as well as the crossover scaling function. Perhaps the first place to look is $g=1/\sqrt{3}$. Maybe it is possible to take advantage of the triangular symmetry of the QBM problem to develop a complete description of the critical fixed point, analogous to the mapping to the three-channel Kondo problem[25] and the three state Potts model[24] that apply in a different regime. In the absence of an analytic solution, this problem is amenable to a numerical Monte Carlo analysis analogous to the calculation of the resonance crossover scaling function performed in Ref. 19.

In addition, there are a number of other fixed points which we did not analyze in detail in this paper. (Recall for $g=1-\epsilon$ we found seven.) It would be of interest to develop a more systematic classification of all of the fixed points, analogous to the analysis of three coupled Luttinger liquids performed by Chamon and co-workers.[39,48]

ACKNOWLEDGMENTS

It is a pleasure to thank Claudio Chamon and Eun-Ah Kim for introducing us to their work and Liang Fu for helpful discussions. This work was supported by NSF under Grant No. DMR-0605066.

APPENDIX: FOUR-TERMINAL CONDUCTANCE

The electrical response of the point contact can be characterized by a four-terminal conductance,

$$I_i = \sum_j G_{ij} V_j, \tag{A1}$$

where I_i is the current flowing into lead i and V_j is the voltage at lead j. In this appendix we will develop a convenient representation for G_{ij}. In the Appendix, Sec. I shows that G_{ij} can be characterized by a 3×3 matrix, whose entries have a clear physical meaning. This representation allows constraints due to symmetry to be expressed in a simple way, which reduces the number of independent parameters characterizing the conductance. Finally, in the Appendix, Sec. III we show how G_{ij} is related to the conductance of the SLL model computed by the Kubo formula.

1. Conductance matrix

The 4×4 matrix G_{ij} is constrained by current conservation to satisfy $\Sigma_i G_{ij}=\Sigma_j G_{ij}=0$. In the absence of any symmetry constraints, there are thus nine independent parameters characterizing G_{ij}. In this section we will cast these nine numbers as a 3×3 matrix, in which each of the entries has a clear physical meaning. In this representation constraints due to symmetry have a simple form.

Since the four currents I_i satisfy $\Sigma_i I_i=0$, they are determined by three *independent* currents, which we define as $I_A=(I_X,I_Y,I_Z)$ and satisfy

$$I_i = \sum_\alpha M_{iA} I_A, \tag{A2}$$

where the 4×3 matrix M_{iA} is

$$M = \frac{1}{2}\begin{pmatrix} 1 & 1 & 1 \\ -1 & 1 & -1 \\ -1 & -1 & 1 \\ 1 & -1 & -1 \end{pmatrix}. \tag{A3}$$

$I_X=I_1+I_4$ is the total current flowing from left to right along the Hall bar, whereas $I_Y=I_1+I_2$ is the current flowing from top to bottom. The third current $I_Z=I_1+I_3$ is the current flowing in on opposite leads (1 and 3) and flowing out in leads 2 and 4. Similarly, the voltages V_i, which are defined up to an additive constant, define three independent voltage differences $V_\beta=(V_X,V_Y,V_Z)$, with

$$V_B = \sum_j M^T_{Bj} V_j. \tag{A4}$$

V_X biases leads 1 and 4 relative to leads 2 and 3, V_Y biases leads 1 and 2 relative to leads 3 and 4, and V_Z biases leads 1 and 3 relative to leads 2 and 4.

The new currents and voltages are then related by a 3×3 conductance matrix,

$$I_A = \sum_\beta G_{AB} V_B. \tag{A5}$$

The nine elements of G_{AB} determine the four-terminal conductance matrix,

$$G_{ij} = \sum_{AB} M_{iA} G_{AB} M^T_{Bj}. \tag{A6}$$

The elements of G_{AB} have a simple physical interpretation. G_{XX} is the "two-terminal" conductance measured horizontally in Fig. 1 by applying a voltage to leads 1 and 4 and measuring the current I_1+I_4. Similarly G_{YY} is a two-terminal conductance measured vertically. G_{ZZ} describes a two-terminal conductance defined by combining the opposite leads 1 and 3 together into a single lead (and similarly for leads 2 and 4). G_{XY} is a skew conductance describing the current I_1+I_4 in response to voltages applied to leads 1 and 2. The other off-diagonal conductances can be understood similarly.

2. Symmetry constraints

The form of G_{AB} simplifies considerably in the presence of symmetries.

a. Time-reversal symmetry

In the presence of time-reversal symmetry the four-terminal conductance obeys the reciprocity relation,[40] $G_{ij}=G_{ji}$. This implies $G_{AB}=G_{BA}$. Thus, with time-reversal symmetry the conductance has six independent components.

b. Spin rotational symmetry

When the spin S_z is conserved the current of up and down spins flowing into the junction must independently be conserved. It follows that

$$I_{1,\mathrm{in}} + I_{3,\mathrm{in}} = I_{2,\mathrm{out}} + I_{4,\mathrm{out}},$$

$$I_{2,\mathrm{in}} + I_{4,\mathrm{in}} = I_{1,\mathrm{out}} + I_{3,\mathrm{out}}. \tag{A7}$$

Since in the Fermi liquid lead (where the interactions have been turned off) we have $I_{i,\mathrm{in}}=(e^2/h)V_i$, this implies that

$$I_1 + I_3 = -I_2 - I_4 = \frac{e^2}{h}(V_1 + V_3 - V_2 - V_4). \tag{A8}$$

It then follows that

$$G_{ZZ} = 2e^2/h,$$

$$G_{ZX} = G_{ZY} = 0. \tag{A9}$$

Thus, with spin conservation the conductance is characterized by three components: the two-terminal conductances G_{XX}, G_{YY} and the skew conductance G_{XY}.

The quantization of G_{ZZ} and vanishing of G_{ZB} are therefore a diagnostic for the conservation of spin. Though spin-orbit terms violating S_z conservation are generically present,

we will argue that at the low energy fixed points of physical interest the conservation of spin is restored.

c. Mirror symmetry

If the junction has a mirror symmetry under interchanging leads $(1,2)\leftrightarrow(3,4)$ or $(1,4)\leftrightarrow(2,3)$, it follows that

$$G_{XY}=0. \tag{A10}$$

Though mirror symmetry is not generically present in a point contact we will argue that that symmetry is restored in the low energy fixed points of interest. Moreover, the *crossover* between the critical fixed point and the stable fixed point described by Eq. (1.1) is also along a line with mirror symmetry. Thus the crossover conductance is characterized by *two* parameters, G_{XX} and G_{YY}, which are simply the two-terminal conductances.

d. Critical conductance

At the transition, where the point contact is just being pinched off the two-terminal conductances must be equal,

$$G_{XX}=G_{YY}\equiv G^*. \tag{A11}$$

In addition, we will argue that this fixed point also has spin rotational symmetry and mirror symmetry. Thus, the critical four-terminal conductance G_{ij} depends on a *single* parameter G^*.

3. Relation to Kubo conductance

In this section we relate the conductance matrix G_{AB} to the conductances of the SLL model, which can be computed with the Kubo formula. There are two issues to be addressed. First is to translate G_{AB} into the spin and charge conductances of the SLL model. Second, we must relate the physical conductance measured with leads to the conductance computed with the Kubo formula. The Kubo conductance describes the response of an infinite Luttinger liquid, where the limit $L\to\infty$ is taken *before* $\omega\to 0$. This does not take into account the contact resistance between the Luttinger liquid and the electron reservoir where the voltage is defined. An appropriate model to account for this is to consider a 1D model for the leads in which the Luttinger parameter $g=1$ for $x>L$.[35,36]

In this section we assume time-reversal symmetry and that spin is conserved. In this case we may define the charge and spin currents in the Fermi liquid leads $(x>L)$ to be

$$I_\rho = I_{1,\mathrm{in}} + I_{4,\mathrm{in}} - I_{1,\mathrm{out}} - I_{4,\mathrm{out}},$$

$$I_\sigma = I_{1,\mathrm{in}} - I_{4,\mathrm{in}} + I_{1,\mathrm{out}} - I_{4,\mathrm{out}}. \tag{A12}$$

Similarly, we define charge and spin voltages,

$$V_\rho = (V_1 + V_4 - V_2 - V_3)/2,$$

$$V_\sigma = (V_1 - V_4 + V_2 - V_3)/2. \tag{A13}$$

These are related by the conductance matrix

$$I_\alpha = G_{\alpha\beta}V_\beta, \tag{A14}$$

where $\alpha,\beta=\rho,\sigma$. By comparing Eqs. (A5) and (A14) it is clear that

$$G_{XX}=G_{\rho\rho},$$

$$G_{YY}=2e^2/h-G_{\sigma\sigma},$$

$$G_{XY}=G_{\rho\sigma}=-G_{\sigma\rho}. \tag{A15}$$

$G_{\alpha\beta}$ can be computed using the Kubo formula using the model in which the interactions are turned off for $x>L$. It is useful, however, to relate this to the Kubo conductance $G^K_{\alpha\beta}$ of an infinite Luttinger liquid. This can be done by relating the voltage $V_{\alpha=\rho,\sigma}$ of the Fermi liquid leads with $g_\rho=g_\sigma=1$ to the voltage $\bar{V}_\alpha$ of the incoming chiral modes of the Luttinger liquid with $g_\rho=g$ and $g_\sigma=1/g$. By matching the boundary conditions at $x=L$ this contact resistance has the form

$$\tilde{V}_\alpha - V_\alpha = R^c_{\alpha\beta}I_\beta \tag{A16}$$

with

$$R^c_{\alpha\beta}=\frac{h}{e^2}\frac{g_\alpha-1}{2g_\alpha}\delta_{\alpha\beta}. \tag{A17}$$

The Kubo formula with infinite leads relates $I_\alpha=G^K_{\alpha\beta}V_\beta$. Eliminating $\bar{V}_\alpha$ from Eqs. (A16) and (A17) gives the matrix relation[39]

$$G_{\alpha\beta}=[(I-R_cG^K)^{-1}G^K]_{\alpha\beta}. \tag{A18}$$

When there is mirror symmetry, so that $G_{XY}=\mu_{\rho\sigma}=0$, the conductance matrix is diagonal, so that Eq. (A18) simplifies. In that case we find

$$G_{XX}=\frac{G^K_{\rho\rho}}{1-R_{\rho\rho}G^K_{\rho\rho}},$$

$$G_{YY}=2\frac{e^2}{h}-\frac{G^K_{\sigma\sigma}}{1-R_{\sigma\sigma}G^K_{\sigma\sigma}}. \tag{A19}$$

[1] C. L. Kane and E. J. Mele, Phys. Rev. Lett. **95**, 226801 (2005).
[2] B. A. Bernevig and S. C. Zhang, Phys. Rev. Lett. **96**, 106802 (2006).
[3] C. L. Kane and E. J. Mele, Phys. Rev. Lett. **95**, 146802 (2005).
[4] F. D. M. Haldane, Phys. Rev. Lett. **61**, 2015 (1988).
[5] B. A. Bernevig, T. L. Hughes, and S. C. Zhang, Science **314**, 1757 (2006).
[6] M. König, S. Wiedmann, C. Brüne, A. Roth, H. Buhmann, L. Molenkamp, X. L. Qi, and S. C. Zhang, Science **318**, 766 (2007).
[7] C. Brüne, A. Roth, E. G. Novik, M. König, H. Buhmann, E. M. Hankiewicz, W. Hanke, J. Sinova, and L. W. Molenkamp, arXiv:0812.3768 (unpublished);A. Roth, C. Brüne, H. Buh-

mann, L. W. Molenkamp, J. Maciejko, X. L. Qi, and S. C. Zhang, arXiv:0905.0365 (unpublished);
[8] C. Wu, B. A. Bernevig, and S. C. Zhang, Phys. Rev. Lett. **96**, 106401 (2006).
[9] C. Xu and J. E. Moore, Phys. Rev. B **73**, 045322 (2006).
[10] C. Y. Hou, E. A. Kim, and C. Chamon, Phys. Rev. Lett. **102**, 076602 (2009).
[11] A. Ström and H. Johannesson, Phys. Rev. Lett. **102**, 096806 (2009).
[12] J. Maciejko, C. Liu, Y. Oreg, X. L. Qi, C. Wu, and S. C. Zhang, arXiv:0901.1685 (unpublished).
[13] Y. Tanaka and N. Nagaosa, arXiv:0904.1453 (unpublished).
[14] K. T. Law, C. Y. Seng, P. A. Lee, and T. K. Ng, arXiv:0904.2262 (unpublished).
[15] A. Furusaki and N. Nagaosa, Phys. Rev. B **47**, 4631 (1993).
[16] C. L. Kane and M. P. A. Fisher, Phys. Rev. B **46**, 15233 (1992).
[17] Here our definition of g_ρ and g_σ differs by a factor of 2 from Ref. 16.
[18] C. L. Kane and M. P. A. Fisher, Phys. Rev. Lett. **68**, 1220 (1992).
[19] K. Moon, H. Yi, C. L. Kane, S. M. Girvin, and M. P. A. Fisher, Phys. Rev. Lett. **71**, 4381 (1993).
[20] F. P. Milliken, C. P. Umbach, and R. A. Webb, Solid State Commun. **97**, 309 (1996).
[21] C. L. Kane and M. P. A. Fisher, Phys. Rev. B **46**, 7268 (1992).
[22] P. Fendley, A. W. W. Ludwig, and H. Saleur, Phys. Rev. Lett. **74**, 3005 (1995); P. Fendley and H. Saleur, Phys. Rev. B **54**, 10845 (1996).
[23] J. L. Cardy, Nucl. Phys. B **240**, 514 (1984).
[24] I. Affleck, M. Oshikawa, and H. Saleur, Nucl. Phys. B **594**, 535 (2001).
[25] H. Yi and C. L. Kane, Phys. Rev. B **57**, R5579 (1998); H. Yi, *ibid.* **65**, 195101 (2002).
[26] A. W. W. Ludwig and I. Affleck, Nucl. Phys. B **428**, 545 (1994).
[27] K. A. Matveev, D. Yue, and L. I. Glazman, Phys. Rev. Lett. **71**, 3351 (1993); D. Yue, L. I. Glazman, and K. A. Matveev, Phys. Rev. B **49**, 1966 (1994).
[28] A. Schmid, Phys. Rev. Lett. **51**, 1506 (1983).
[29] M. P. A. Fisher and W. Zwerger, Phys. Rev. B **32**, 6190 (1985).
[30] F. Guinea, V. Hakim, and A. Muramatsu, Phys. Rev. Lett. **54**, 263 (1985).
[31] In Ref. 16 $\tilde{\theta}_{\sigma,\rho}$ was referred to as $\varphi_{\sigma,\rho}$. To avoid confusion with the φ_σ in Sec. II B 5 we follow the notation in Ref. 24.
[32] A. O. Caldeira and A. J. Leggett, Ann. Phys. **149**, 374 (1983).
[33] K. Itai, Phys. Rev. Lett. **58**, 602 (1987).
[34] G. T. Zimanyi, K. Vladar, and A. Zawadowski, Phys. Rev. B **36**, 3186 (1987).
[35] D. L. Maslov and M. Stone, Phys. Rev. B **52**, R5539 (1995).
[36] I. Safi and H. J. Schulz, Phys. Rev. B **52**, R17040 (1995).
[37] V. V. Ponomarenko, Phys. Rev. B **52**, R8666 (1995).
[38] A. Kawabata, J. Phys. Soc. Jpn. **65**, 30 (1996).
[39] C. Chamon, M. Oshikawa, and I. Affleck, Phys. Rev. Lett. **91**, 206403 (2003); M. Oshikawa, C. Chamon, and I. Affleck, J. Stat. Mech.: Theory Exp. (2006) 02008.
[40] M. Büttiker, Phys. Rev. Lett. **57**, 1761 (1986).
[41] K. D. Schotte and U. Schotte, Phys. Rev. **182**, 479 (1969).
[42] C. L. Kane, K. A. Matveev, and L. I. Glazman, Phys. Rev. B **49**, 2253 (1994).
[43] L. I. Glazman, I. M. Ruzin, and B. I. Shklovskii, Phys. Rev. B **45**, 8454 (1992).
[44] A similar estimate was given in Ref. 12 without the numerical factor in the logarithm.
[45] M. König, H. Buhmann, L. W. Molenkamp, T. Hughes, C.-X. Liu, X.-L. Qi, and S.-C. Zhang, J. Phys. Soc. Jpn. **77**, 031007 (2008).
[46] L. J. Cooper, N. K. Patel, V. Drouot, E. H. Linfield, D. A. Ritchie, and M. Pepper, Phys. Rev. B **57**, 11915 (1998).
[47] C. Liu, T. L. Hughes, X. L. Qi, K. Wang, and S. C. Zhang, Phys. Rev. Lett. **100**, 236601 (2008).
[48] C. Y. Hou and C. Chamon, Phys. Rev. B **77**, 155422 (2008).